Chemical Geology 636 (2023) 121645

Contents lists available at ScienceDirect

Chemical Geology

journal homepage: www.elsevier.com/locate/chemgeo

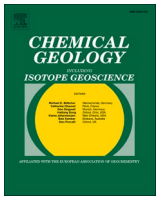

The effect of platinum-group minerals on differentiation of platinum-group elements in magmatic sulfide deposits: Evidence from the Cu-Ni-PGE deposits in the Yangliuping area of the Emeishan large igneous province, SW China

Qing-Lin Liang [a,*], Xie-Yan Song [a], Ting-Mao Long [a], Richard Wirth [b], Zhi-Hui Dai [a]

[a] State Key Laboratory of Ore Deposit Geochemistry, Institute of Geochemistry, Chinese Academy of Sciences, Guiyang, PR China
[b] German Research Centre for Geosciences GFZ, 3.5 Interface Geochemistry, Telegrafenberg, Potsdam, Germany

ARTICLE INFO

Editor: Marco Fiorentini

Keywords:
Platinum-group minerals
Platinum-group elements
Differentiation
Cu-Ni-PGE deposits
Yangliuping
Emeishan

ABSTRACT

Platinum-group minerals (PGM) are important host phases for platinum-group elements (PGE) in magmatic sulfide deposits. Recent studies have demonstrated that some PGM, such as sperrylite, can crystallize early from sulfide liquids. It is important to determine whether and how these PGM particles affect the enrichment and differentiation of PGE in Cu-Ni-PGE deposits. The magmatic sulfide deposits in the Yangliuping area (mainly consisting of the Yangliuping deposit and Zhengziyanwo deposit) are the largest Cu-Ni-PGE deposits in the Emeishan large igneous province, SW China. Primitive-mantle normalized PGE patterns and fractional crystallization modelling show that massive ores in the Yangliuping deposit are enriched in Pd and Pt. In contrast, massive ores, breccia ores and Cu-rich ores in the Zhengziyanwo deposit are depleted in Pt. Scanning electron microscopy (SEM), laser ablation inductively coupled plasma mass spectrometry (LA-ICP-MS), focused ion beam (FIB) and transmission electron microscopy (TEM) were used to constrain the occurrence of PGE in the massive ores from the two deposits. Mass balance calculation shows that <7% of Ir, Rh and Pt occur in base metal sulfides (BMS, mainly pyrrhotite, pentlandite and chalcopyrite) as solid solution in both the Yangliuping and Zhengziyanwo massive ores. 17% and 91% Pd are present in solid solution within BMS in the Yangliuping and Zhengziyanwo massive ores, respectively. In the Yangliuping massive ores, $PtAs_2$ and Pd-PGM particles were commonly found within BMS crystals, and Ir-Rh-(Pt) sulfarsenides enclosed in cobaltite-gersdorffite solid solution (CGSS) are enriched in Pt. In contrast, in the Zhengziyanwo massive ores, no $PtAs_2$ particles and fewer Pd-PGM particles were found, and Ir-Rh-(Pt)AsS particles enclosed in CGSS are poor in Pt. The distribution, mineralogy and microstructures of Ir-Rh-(Pt)AsS, $PtAs_2$ and Pd-PGM particles in both the Yangliuping and Zhengziyanwo deposits suggest that they mainly crystallized from sulfide liquids or formed from Pd-Pt-semimetal-rich droplets. We suggest that the incorporation of Pd-PGM and $PtAs_2$ particles into MSS cumulates led to the enrichment of Pd and Pt in the Yangliuping massive ores. In the Zhengziyanwo deposit, early fractional crystallization of $PtAs_2$ reduced the Pt content in sulfide liquids and resulted in the formation of Pt-depleted sulfide ores and low-Pt Ir-Rh-(Pt)AsS particles, but no Pt-rich sulfide ores have been found to date. As a result, the role of PGM particles should be considered when using PGE to trace the formation process of Cu-Ni-PGE deposits. This study also provides additional evidence that the behavior of Pt in sulfide liquids is influenced by thermodynamic conditions and As, and suggests a potential for Pt-rich sulfide ores exploration in the Zhengziyanwo deposit.

1. Introduction

Platinum-group elements (PGE) are widely used in tracing various geological processes, such as the origin and evolution of mantle-derived silicate melts and the formation of magmatic sulfide deposits (Barnes and Ripley, 2016; Harvey and Day, 2016). Magmatic sulfide deposits,

* Corresponding author at: Institute of Geochemistry, Chinese Academy of Sciences, PR China.
E-mail address: liangqinglin@mail.gyig.ac.cn (Q.-L. Liang).

https://doi.org/10.1016/j.chemgeo.2023.121645
Received 7 April 2023; Received in revised form 16 July 2023; Accepted 29 July 2023
Available online 31 July 2023

including Cu-Ni-PGE deposits and PGE deposits, are formed by the accumulation of sulfide droplets segregated from mantle-derived mafic-ultramafic magma (Naldrett, 2004; Barnes and Lightfoot, 2005). In magmatic sulfide deposits, PGE are hosted by base metal sulfides (BMS, mainly pyrrhotite, pentlandite and chalcopyrite) or occur as individual platinum-group minerals (PGM) (Cabri et al., 1981; Cabri and Laflamme, 1984; Barnes et al., 2008; Dare et al., 2010a; Chen et al., 2015), which are alloys or compounds of PGE, S and semimetals (As, Sn, Sb, Te and Bi) (Cabri, 1981, 2002; O'Driscoll and González-Jiménez, 2016). Some PGM, such as sperrylite ($PtAs_2$) and irarsite-hollingworthite-platarsite solid solution ((Ir-Rh-Pt)AsS), have crystallized from silicate melts (Wirth et al., 2013; Barnes et al., 2016; González-Jiménez et al., 2018, 2019) and sulfide liquids (Dare et al., 2010a; Helmy et al., 2013; Helmy and Bragagni, 2017; Liang et al., 2022). Understanding the effects of PGM particles migration on the enrichment and differentiation of PGE in magmatic sulfide deposits is crucial for improving our knowledge of PGE behavior and tracing the formation processes of magmatic sulfide deposits.

The role of the migration of PGM particles on the enrichment and differentiation of PGE has been extensively studied in PGE deposits and mafic-ultramafic intrusions (Ballhaus and Sylvester, 2000; McDonald, 2008; Wirth et al., 2013; Maier et al., 2015). Recent experimental and empirical studies have shown that PGM particles crystallized in silicate melts can be incorporated into sulfide liquids (Anenburg and Mavrogenes, 2016, 2020; Kamenetsky and Zelenski, 2020). This process is believed to play a significant role in the enrichment of PGE in PGE deposits hosted in layered mafic-ultramafic sills (Tredoux et al., 1995; Ballhaus et al., 2000; Wirth et al., 2013; Junge et al., 2014; González-Jiménez et al., 2018). On the other hand, the enrichment of Pt in the Monts de Cristal Complex was attributed to the cumulation of $PtAs_2$ particles crystallized from silicate melts (Maier et al., 2015; Barnes et al., 2016). Similarly, the depletion of Pt in high-Mg Pual Ridge lave was linked to the fractional crystallization of Pt-rich alloys (Park et al., 2013). Furthermore, it has been recognized that $PtAs_2$ crystallized early from sulfide liquids (prior or simultaneously to the crystallization of MSS) in the Platreef and Merensky Reef, Bushveld Complex (Junge et al., 2014) and the Main Sulfide Zone, Great Dyke (Coghill and Wilson, 1993). The detachment of $PtAs_2$ particles from sulfide liquids and their subsequent capture by growing olivine crystals is believed to be the key process in developing the PGE mineralization in ultramafic complexes at western Andriamena, Madagascar (Ohnenstetter et al., 1999; McDonald, 2008).

In the case of Cu-Ni-PGE deposits, there is consensus that the fractional crystallization of MSS differentiates the IPGE and Rh from Pd and Pt, forming IPGE-Rh-Ni-rich massive ores and Pd-Pt-Cu-rich ores (Keays and Crocket, 1970; Naldrett et al., 1992, 1996; Barnes et al., 1997; Mungall et al., 2005; Liu and Brenan, 2015; Mansur et al., 2019b). However, massive ores that show negative Pt anomalies in primitive-mantle normalized patterns have been found in many deposits, such as the Jinchuan deposit (Song et al., 2009; Chen et al., 2013), the Tamarack deposit (Smith et al., 2022), the Nova-Bollinger and Black Swan deposits (Barnes, 2004; Barnes et al., 2022), and the Creighton deposit at Sudbury and the Alexo deposit (Barnes and Naldrett, 1986; Dare et al., 2010b). Different interpretations have been proposed to explain the depletion of Pt in massive ores. For instance, it was proposed that the early fractional crystallization of $PtAs_2$ or Fe-Pt alloy in sulfide liquids resulted in the depletion of Pt in massive ores (Song et al., 2009; Smith et al., 2022). Others proposed that the migration of Pt-Cu-rich residual sulfide liquids after Pd has diffused into pentlandite (Chen et al., 2013) or the selective leaching of Pt by fluids during hydrothermal alteration (Su et al., 2008) could have caused the depletion of Pt in massive ores. Additionally, Pt depletion in massive ores may be associated with nugget effects (Savard et al., 2010), where most samples without nuggets contain very low Pt concentrations, whereas a small number containing nuggets show anomalous high concentration (Barnes et al., 2022). These interpretations mentioned above were proposed primarily based on whole-rock PGE data and Monte Carlo simulation. To determine whether and how Pt-PGM particles affect Pt differentiation in Cu-Ni-PGE deposits, combined studies of PGE occurrences and whole-rock geochemistry are needed.

The Cu-Ni-PGE deposits in the Yangliuping area (mainly consisting of the Yangliuping deposit and Zhengziyanwo deposit) are the largest magmatic sulfide deposits in the Emeishan large igneous province (ELIP) containing about 0.5 million tons Ni, 0.17 million tons Cu and 55 tons PGE with average grade of 0.45 wt%, 0.16 wt% and 0.5 ppm, respectively (BGMS, 1982; Song et al., 2003). Nanometer to micrometer-sized Ir-Rh-(Pt)AsS, $PtAs_2$, Pd-PGM and cobaltite-gersdorffite solid solution (CGSS) particles were found within pyrrhotite, pentlandite and chalcopyrite crystals in sulfide ores from the two deposits (Song et al., 2004; Liang et al., 2019). These particles mainly exhibit a euhedral shape with some displaying zoned textures, which were suggested to have crystallized from sulfide liquids (Liang et al., 2019). The Cu-Ni-PGE deposits at the Yangliuping area are ideal targets for studying the effects of PGM particles migration. This study analyzed whole-rock PGE concentrations of different types of sulfide ores from the Yangliuping and Zhengziyanwo deposits. PGE occurrences in BMS of massive ores and Cu-rich ores from the two deposits were analyzed using SEM, LA-ICP-MS, FIB and TEM. These data were used to discuss the effects of $PtAs_2$ and Pd-PGM particles migration on the enrichment and differentiation of PGE in the Yangliuping and Zhengziyanwo deposits, its implication for the behavior of PGE in sulfide liquids and Pt-rich sulfide ore exploration.

2. Geological background

The Emeishan Large Igneous Province (ELIP) (~260 Ma) located in South-Western China is comprised of late Permian continental flood basalts and numerous contemporaneous mafic-ultramafic intrusions. The flood basalts cover an area of over 0.5 million km^2 and are up to 5 km thick (Song et al., 2001; Xu et al., 2001). Two types of mafic-ultramafic intrusions have been found within the ELIP. Layered intrusions hosting giant V-Ti magnetite ore deposits, such as the Panzhihua, Hongge, Baima and Taihe deposits, are located in the central ELIP (Zhong et al., 2002; Song et al., 2013). Sill-like mafic-ultramafic intrusions hosting magmatic sulfide deposits, such as the Yangliuping, Qingkuangshan and Zhubu deposits, were found in the western ELIP (Song et al., 2003; Wang and Zhou, 2006; Tao et al., 2008).

In the Yangliuping area, north-western corner of the ELIP, four mineralized sills were found in a dome structure consisting of Devonian-Permian strata (Fig. 1A) (Song et al., 2003). Both the Yangliuping and Zhengziyanwo sills were emplaced in Devonian and Carboniferous schist and marble. The Yangliuping sill, which is 2600 m in length and up to 254 m in thickness, hosts the Yangliuping deposit. The Zhengziyanwo sill, which is 2100 m in length and up to 298 m in thickness, hosts the Zhengziyanwo deposit. The sills are well fractionated and experienced strong post-magmatic alteration. From the bottom to the top, they were classified into serpentinite, talc schist, tremolite and altered gabbro (Figs. 1B-C), which correspond to the protoliths of peridotite, olivine websterite, olivine clinopyroxenite and gabbro, respectively (Song et al., 2003). Many lenticular carbonate xenoliths, ranging in length from 10 cm to 30 m, were found in the mineralized sills (BGMS, 1982; Song et al., 2003; Song, 2004).

The sulfide ore bodies are restricted to the lower parts of the serpentinite in the Yangliuping and Zhengziyanwo sills. The disseminated ore bodies of both the Yangliuping and Zhengziyanwo deposits are >1000 m in length and up to 120 m in thickness containing >90% of the Ni, Cu and PGE reserves. Massive ores were mainly found at the base of the sills with sulfide contents decreasing upward and grading into net-textured ores (classified as densely disseminated ores in Song, 2004) and disseminated ores (Fig. 1B). The largest massive orebody was found in the Yangliuping deposit, which is irregular lenticular and about 200 m in length and up to 20 m in thickness. It is mainly parallel to the footwall rock contact and locally extends into the footwall rocks. The massive

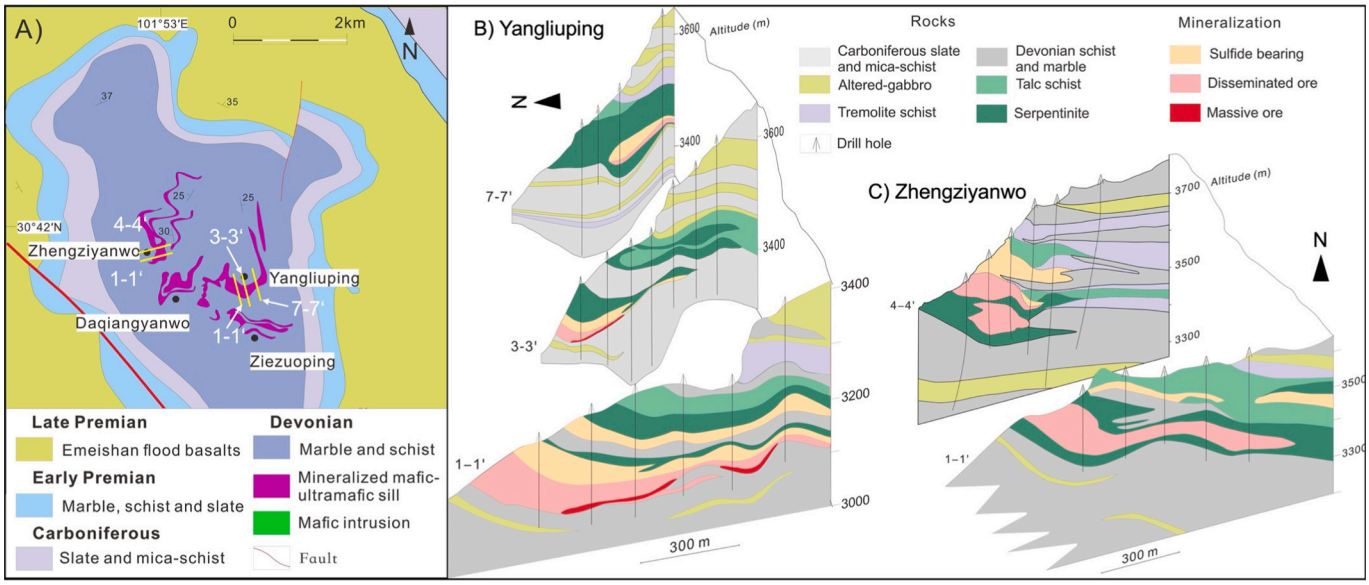

Fig. 1. A. Geological map of the Yangliuping tectonic dome, southwestern China, showing the distribution of mafic-ultramafic sills. B-C. Cross sections (the positions are annotated as yellow lines in Fig. 1A) of the Yangliuping (B) and Zhengziyanwo (C) sills. Modified from BGMS (1982). (For interpretation of the references to colour in this figure legend, the reader is referred to the web version of this article.)

orebodies in the Zhengziyanwo deposit are less common and smaller compared to the Yangliuping deposit. The largest is only about 40 m in length, 20 m in width and 4 m in thickness. Some irregular massive orebodies (<20 m long and 5 m thick) were also found in the footwall rocks below the two sills. These irregular orebodies commonly are partially connected to the net-textured ores at the base of the sills (Song et al., 2003; Song, 2004). In the Zhengziyanwo deposit, Cu-rich ores were found in the marble xenoliths and marble wall-rock (BGMS, 1982).

3. Samples and analytical methods

3.1. Sample description

In total 62 samples were collected from the Yangliuping deposit (33 samples) and the Zhengziyanwo deposit (29 samples) (Table S1). One representative thin section and block of each sample was studied using conventional optical microscopy at the Institute of Geochemistry, Chinese Academy of Sciences (IGCAS).

Disseminated ores contain 1–26 vol% sulfides while net-textured ores contain 27–55 vol% sulfides. The proportions of pyrrhotite, pentlandite and chalcopyrite are similar in both ores with a ratio of approximately 70:10:20. Cumulate silicates in these ores were highly

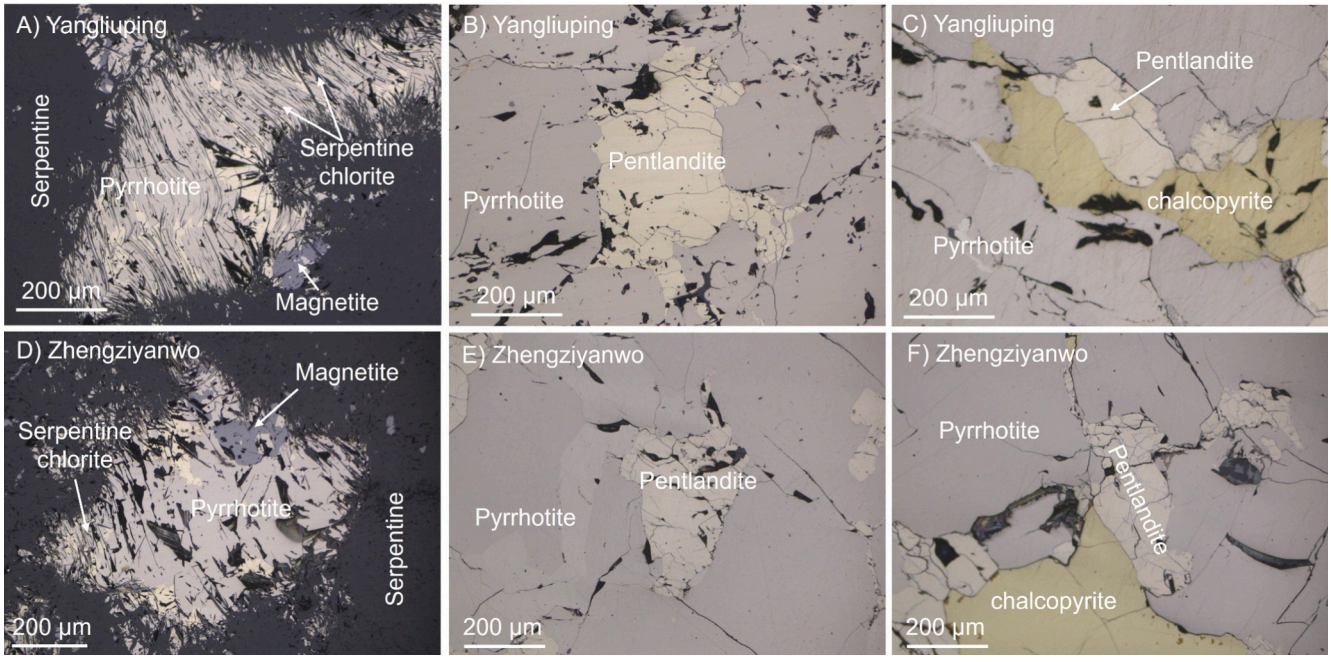

Fig. 2. Reflected light micrographs of disseminated ores (A, D) and massive ores (B-C, E-F) from the Yangliuping deposit (A-C) and the Zhengziyanwo deposit (D-F), respectively.

altered, without remnants of primary olivine and pyroxene. Serpentine and tremolite show pseudomorphs after olivine and pyroxene, and sulfides are interstitial to these pseudomorphs. Serpentine and chlorite grains were found embedded in sulfide minerals, and minor amount of anhedral magnetite were observed around altered chalcopyrite or pyrrhotite grains (Figs. 2A, D).

The massive ores from the Yangliuping and Zhengziyanwo deposits show similar mineralogical characteristics. It commonly contains 70–95 vol% sulfides with a lower proportion of chalcopyrite compared to the disseminated ores and net-textured ores. The sulfides in massive ores generally consist of 50–70% pyrrhotite, 10–25% pentlandite and <5% chalcopyrite, and no magmatic euhedral magnetite were found. Pyrrhotite occurs as anhedral centimeter-sized patches, while pentlandite commonly forms anhedral polycrystalline aggregates (Figs. 2B, E) and is sometimes found at the boundaries between chalcopyrite and pyrrhotite (Fig. 2C, F). Minor flame-like pentlandite was also found along fractures or edges of pyrrhotite grains. Chalcopyrite occurs as anhedral grains randomly dispersed between pyrrhotite and pentlandite grains (Figs. 2C, F). One massive ore in the Yangliuping deposit contains about 48% chalcopyrite, which occurs as a vein (about 1 cm in width) penetrating MSS cumulates. Secondary magnetite, pyrite and millerite grains were not found in massive ores from the Yangliuping and Zhengziyanwo deposits (Figs. 2B-C, E-F).

Breccia ores and Cu-rich ores were also collected from the Zhengziyanwo deposit (Table S1). The breccia ores contain 30–56 vol% sulfides, which appear as veins penetrating the wall rocks (Fig. S1A). The sulfides are mostly pyrrhotite and pentlandite with <2% chalcopyrite (Fig. S1B). The Cu-rich ores contain 17–81 vol% sulfides with up to 87% chalcopyrite (Fig. S1C).

3.2. Analytic methods

Whole-rock S, Ni, Cu and semimetal elements were measured at the Mineral-ALS Chemex (Guangzhou) Co., Ltd. Details of the methodologies can be found in Liang et al. (2022).

Whole-rock PGE compositions were measured using isotope dilution inductively coupled plasma mass spectrometry (ID-ICP-MS) with an improved digestion technique developed by Qi et al. (2011) at the IGCAS. About 300 g of each sample was pulverized to 200 mesh. 1–3 g powder of massive ores and 5–8 g powder of disseminated ores were dissolved in HF and HNO_3 in polytetrafluoroethylene (PTFE) beaker to remove sulfides and silicates. Then, the dried residual was dissolved in HF + HNO_3 at 190 °C for 48 h. The PGE within the final solution were collected using a Te-coprecipitation method. Sample accuracy was checked internally using Certified Reference Materials (CRM) WPR-1, UMT-1 and WMG-1. Meanwhile, duplicated CRMs and samples were also analyzed. Based the CRMs data, the relative standard uncertainties for Ir, Ru, Rh, and Pt range from 0.5% to 3.7%, while for Pd it ranges from 3.3% to 7.6% (Table S2).

According to the whole-rock data, 4 massive ores from the Yangliuping deposit, 3 massive ores and 2 Cu-rich ores from the Zhengziyanwo deposit enriched in PGE were selected (Table S1) for further scanning electron microscopy (SEM) and laser ablation inductively coupled plasma mass spectrometry (LA-ICP-MS) studies. The whole block of these massive ores was mapped (back-scattered electron-mapping) using a FEI Scios SEM. PGM show brighter contrast compared to BMS in the backscattered electron (BSE) images. PGM particles were identified offline and then analyzed using the FEI Scios SEM at the IGCAS. The detection limit for PGE by SEM-EDX analyses is about 0.07 at.% (~0.3 wt%) (Wirth et al., 2013).

PGE and semimetals concentrations in BMS of the massive ores and Cu-rich ores were measured using an Agilent 7700× quadrupole ICP-MS coupled to an ASI RESOLution-LR-S155 laser microprobe at the IGCAS. The concentrations of PGE and semimetals were measured separately (separate locations) to improve the quality of the concentration data. A laser beam spot size of 26 μm (in diameter) was used for the measurements with a fluence of 3 J/cm^2 and a pulse rate of 5 Hz. Ablations were performed in He atmosphere with a 0.35 L/min flowrate. The ablated aerosol was mixed with Ar (1.05 L/min) as transport gas. ^{57}Fe was used for internal standardization and MASS-1 was used to monitor the results. The certified reference standards STDGL3, Po725 and GED-1 g were used for external calibration of the PGE and semimetals. The data of these certified reference standards can be found in Table S3. The following isotopes were measured: ^{34}S, ^{55}Mn, ^{57}Fe, ^{59}Co, ^{60}Ni, ^{65}Cu, ^{66}Zn, ^{75}As, ^{77}Se, ^{93}Nb, ^{99}Ru, ^{103}Rh, ^{106}Pd, ^{109}Ag, ^{111}Cd, ^{118}Sn, ^{121}Sb, ^{125}Te, ^{185}Re, ^{189}Os, ^{193}Ir, ^{195}Pt, ^{197}Au, ^{206}Pb, ^{209}Bi. Meanwhile, ^{87}Sr, ^{90}Zr, ^{92}Zr, ^{181}Ta were monitored to handle potential interferences. Oxidation yield ThO/Th < 0.1 was an important tuning parameter to ensure a low production of oxides interferences. During the analyses, ^{29}Si and ^{45}Sc in quartz (in-house standard) were analyzed three times per hour to confirm the contribution of oxygen. Total acquisition time for each analysis was 90 s, comprising 30 s for gas background and 60 s for ablation signal measurement. The details about the methods used for calibration and interferences correction (Longerich et al., 1996; Kosler, 2001; Cabri et al., 2017) can be found in Liang et al. (2019, 2022).

The microstructure of platinum-group minerals was analyzed using FIB-TEM techniques. The foils were prepared using a FEI Scios FIB at the IGCAS. The microstructure of platinum-group minerals was then analyzed using a FEI Tecnai G2 F20 TEM equipped with a field-emission gun electron source, a Gatan imaging filter GIF™, an EDAX X-ray analyzer and a Fishione high-angle annular dark field (HAADF) detector at the Nanjing University. To avoid collecting Bragg scattered electrons, HAADF images were acquired using a camera length of 75 mm. Inorganic Crystal Structure Database (ICSD) was used in indexing diffraction patterns of platinum-group minerals.

4. Results

4.1. Whole-rock Ni, PGE and semimetals

The primitive mantle-normalized chalcophile elements patterns of the disseminated ores and net-textured ores from the Yangliuping and Zhengziyanwo deposits show an overall increase from Ni to PGE and Cu (Figs. 3A-B). The disseminated ores from the Yangliuping deposit have slightly lower Ni and Pt, comparable Pd but higher Ir, Ru, Rh and As tenors (the tenor of the sulfide) on average when compared to the Zhengziyanwo disseminated ores (Fig. 4, Table 1). However, the Yangliuping massive ores have higher Pt and Pd tenors than the Zhengziyanwo massive ores (Figs. 3C-D).

In the Yangliuping deposit, the massive ores have similar Pd and Pt tenors to the disseminated ores and net-textured ores (Fig. 3C). The disseminated ores, net-textured ores and massive ores have comparable (Pt + Pd)/(Ir + Ru + Rh) ratios (Figs. 5A-D). As for the semimetals, the massive ores have similar As and Te but lower Sb and Bi concentrations compared to the disseminated ores and net-textured ores (Figs. 5A-D).

In the Zhengziyanwo deposit, the massive ores and breccia ores are generally enriched in IPGE and Rh and show strong negative Pt anomalies (Fig. 3D). The Cu-rich ores are enriched in Pd but poor in Pt when compared to the disseminated ores (Fig. 3D). The Co/Ni ratio of the Cu-rich ores varies from 0.03 to 0.04 (Table S1), which falls within the typical range of 0.01–0.5 for magmatic sulfides (Smith et al., 2022 and references therein). The concentrations of semimetals in sulfide ores (except for Cu-rich ores) show a strong correlation with their (Pt + Pd)/(Ir + Ru + Rh) ratios (Figs. 5E-H). The Cu-rich ores have higher Sb, Bi and Te tenors (Figs. 5F-H) but lower As tenor (Fig. 5E) compared to the massive ores.

4.2. PGE and semimetals in base metal sulfides

A total of 95 BMS particles in 4 massive ores from the Yangliuping deposit and total 91 BMS particles in 3 massive ores and 2 Cu-rich ores

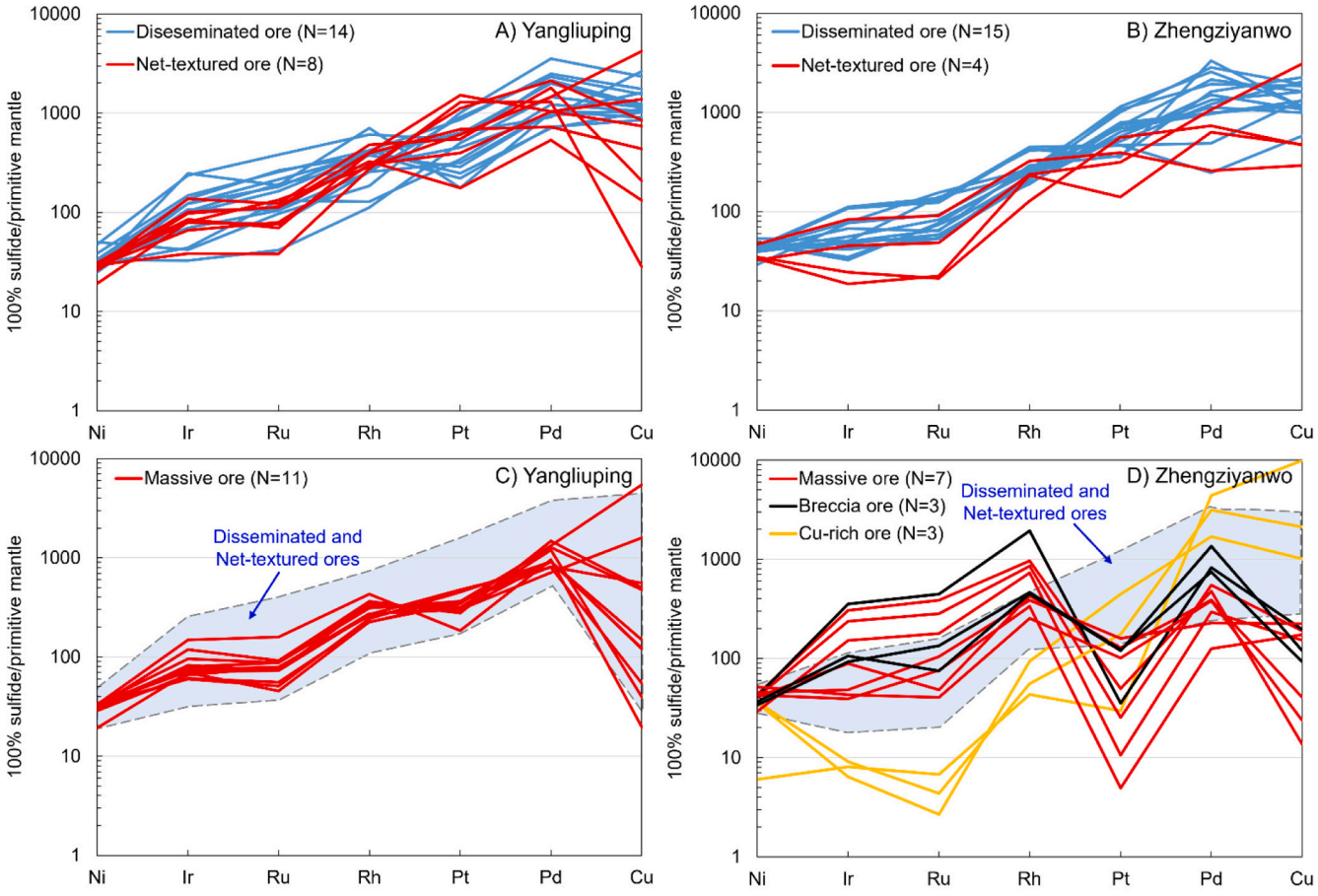

Fig. 3. Primitive-mantle normalized Ni, PGE and Cu (in 100% sulfide) patterns of the sulfide ores from the Yangliuping deposit (A) and the Zhengziyanwo deposit (B). Whole-rock data are from this study, Song et al. (2004) and Liang et al. (2019) as shown in Table S1. Primitive mantle values are from McDonough and Sun (1995) and Barnes and Maier (1999).

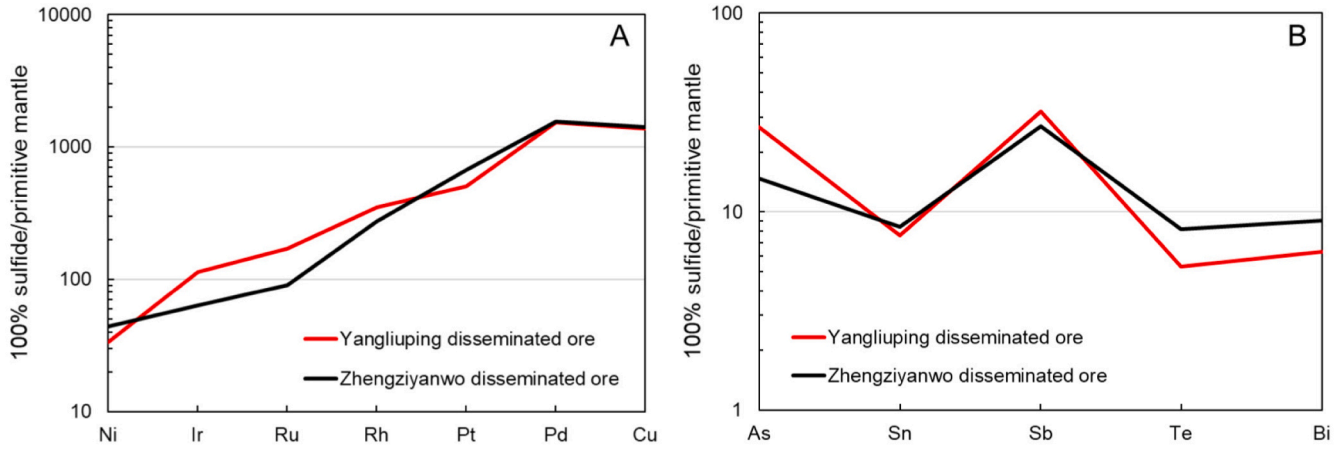

Fig. 4. Primitive-mantle normalized Ni, PGE and Cu (in 100% sulfide) pattern (A) and whole-rock semimetals concentrations (in 100% sulfide) (B) of the average disseminated ores from the Yangliuping and Zhengziyanwo deposits. Whole-rock data are shown in Table S1. Primitive mantle values are from McDonough and Sun (1995) and Barnes and Maier (1999).

from the Zhengziyanwo deposits were analyzed (Table S4). Time-resolved spectra of LA-ICP-MS show flat signals for PGE occurring in BMS as solid solution and show PGE-peaks when PGM or CGSS inclusions were encountered. These PGE-peaks were avoided in the selected integration intervals (Fig. S2).

Thirty-one time-resolved spectra of BMS from Yangliuping massive ores and 27 from Zhengziyanwo massive ores contain IPGE-Rh-(Pt)-peaks. One Os-Ru-Rh-peak was also found in a time-resolved spectrum of pyrrhotite from the Zhengziyanwo Cu-rich ore (Table 2). Most IPGE-Rh-(Pt)-peaks from Yangliuping contain an obvious Pt-peak (Figs. S2A-C), whereas Pt is commonly absent from the PGE-peaks from Zhengziyanwo (Figs. S2E-F) (Table 2).

Table 1
Average whole-rock concentrations of PGE and semimetals (100% sulfide) in sulfide ores from the Yangliuping and Zhengziyanwo deposits.

Deposit	Ore type	N	Ni	Cu	Co	Ir	Ru	Rh	Pt	Pd	As	Sb	Te	Bi
			wt%	wt%	ppm	ppb	ppb	ppb	ppb	ppb	ppm	ppm	ppm	ppm
Yangliuping	Disseminated ore	14	6.55	4.13	3397	385	854	333	3548	6143	27	59	6	7
	Net-textured ore	8	5.44	2.99	1878	290	465	328	5548	4991	10	12	7	8
	Massive ore	11	6.04	2.48	1760	287	401	283	2375	4106	13	1	6	2
Zhengziyanwo	Disseminated ore	15	8.64	4.25	2882	217	454	261	4725	6204	15	30	8	9
	Net-textured ore	4	7.30	3.29	1956	146	229	218	2461	2688	11	6	10	4
	Breccia ore	3	7.42	0.41	1986	625	1090	902	644	3894	21	11	3	3
	Massive ore	7	8.21	0.35	2774	443	796	535	477	1395	11	1	3	2
	Cu-rich ore	3	5.20	13.01	1494	27	23	61	1516	12,268	5	17	11	5

The primary data is shown in Table S1. N = the number of sample.

The full LA-ICP-MS data set is shown in Table S4. The average concentrations of PGE and semimetals in each BMS of the sulfide ores can be found in Table 3. In BMS from the Yangliuping and Zhengziyanwo massive ores, the concentrations of Ir, Rh, and Pt generally vary from undetectable levels to several tens of ppb (Fig. 6), except for the pentlandite and pyrrhotite in one Zhengziyanwo massive ore contain hundreds ppb Ir and Rh (Fig. 6C). The concentration of Pd in pentlandite of the Yangliuping massive ores (about 5 ppm on average) (Fig. 6B) is lower than that of the Zhengziyanwo massive ores (about 7 ppm on average) (Fig. D) (Table 3).

4.3. CGSS and platinum-group minerals

Four massive ores from the Yangliuping deposit, as well as 3 massive ores and 1 Cu-rich ores from the Zhengziyanwo deposits were analyzed (Table S1). Micrometer-sized CGSS, $PtAs_2$, Pd-PGM and nanometer-sized Ir-Rh-(Pt)AsS particles were found in both the Yangliuping and Zhengziyanwo sulfide ores (Table 4). The Pd-PGM consisting of Pd, Sb, Bi and Te were classified into michenerite (PdBiTe), testibiopalladite (PdSbTe), kotulskite (PdTe) based on the chemical compositions of PGM given by Cabri (2002). Nanometer-sized Ir-Rh-(Pt)AsS particles were found in pyrrhotite, pentlandite, chalcopyrite and CGSS crystals (Table 4) (Liang et al., 2019). However, this study mainly focused on the Ir-Rh-(Pt)AsS particles in CGSS crystals.

CGSS particles are mainly enclosed in pyrrhotite, pentlandite, chalcopyrite crystals and less frequently located at BMS grain boundaries or enclosed in altered BMS (Table 4). They show subhedral to euhedral shapes with grain sizes varying from 2 to 20 μm (Figs. 7A-B, D-E). CGSS is an important PGE container in the Cu-Ni-PGE deposits at the Yangliuping area, which contains up to 1.37 wt% Ir, 6.4 wt% Rh and 2.46 wt % Pd (Song et al., 2004; Liang et al., 2019). CGSS enriched in PGE and containing $PtAs_2$ and (Ir-Rh-Pt)AsS inclusions was also found in the Creighton deposit, Sudbury (Dare et al., 2010b), the Spotted Quoll deposit, Western Australia (Prichard et al., 2013a) and the mineralized Talnotry diorite intrusion, Scotland (Power et al., 2004).

A total of 42 nm-sized Ir-Rh-(Pt)AsS particles were found in CGSS crystals from the Yangliuping massive ores, while 37 particles were observed in those from the Zhengziyanwo massive ores (Table 4). These particles are subhedral to euhedral with grain sizes of 300 nm to 1000 nm (up to 2 μm) (Figs. 7A-B, D-E). They were found either in the brighter zone (Fig. 7A) or within the core of CGSS crystals (Figs. 7B, D-E). Most Ir-Rh-(Pt)AsS particles from Yangliuping are enriched in Pt (Table 4), as indicated by a strong Pt$L\alpha$ line at 9.4 keV in the SEM-EDX spectrum (Fig. 7C). However, Pt was not detected in most Ir-Rh-(Pt)AsS particles from Zhengziyanwo (Fig. 7F, Table 4). This is consistent with the characteristics of PGE-peaks in LA-ICP-MS spectra (Fig. S2).

A total of 88 $PtAs_2$ particles were found in the Yangliuping massive ores (Fig. 9A, Table 4). They commonly show euhedral shape and less frequently subhedral to anhedral shapes (Figs. 8A-B, Fig. 9D) with grain sizes of 0.3 to 25 μm. They were mostly enclosed in pyrrhotite, pentlandite, chalcopyrite and CGSS crystals (Fig. 9C). $PtAs_2$ particles within CGSS are typically <1 μm in diameter (up to 2 μm). One particle is partially enclosed by Ir-Rh-(Pt)AsS in CGSS (Fig. 7B). In contrast, $PtAs_2$ is absent from the Zhengziyanwo massive ores (Fig. 9B) and only one subhedral $PtAs_2$ particle with grain size of 10 μm was found within chalcopyrite in the Cu-rich ore (Fig. 8K).

Forty-two PdBiTe, PdSbTe and PdTe particles were found in the Yangliuping massive ores (Fig. 9A), while 21 were found in the Zhengziyanwo massive ores (Fig. 9B) (Table 4). These particles are mainly enclosed in pyrrhotite and chalcopyrite or located at BMS grain boundaries (Fig. 9E), and they are mainly subhedral to anhedral (Figs. 8C-J, Fig. 9F). The Pd-PGM particles occur either as individual (Figs. 8C-F, J) or composite (Figs. 8G-I) grains. The Pd-PGM particles in the Yangliuping massive ores are larger (commonly 2–20 μm and up to 100 μm in long axis) (Figs. 8C-F) than that in the Zhengziyanwo massive ores (0.3–10 μm) (Figs. 8G-J).

One foil was cut across a $PtAs_2$ particle (Fig. 8A) in the Yangliuping massive ore and another was cut across the composite grains of PdTe and PdBiTe (Fig. 8I) in the Zhengziyanwo massive ore. The grain boundary between PdTe and PdBiTe is sharp and they are located completely within pyrrhotite crystals (Fig. 10B). These PGM particles exhibit anhedral to subhedral shapes with grain sizes ranging from 3 to 5 μm and show no preferred orientation relationship with the host pyrrhotite (Fig. 10).

5. Discussion

5.1. The effect of hydrothermal alteration

During hydrothermal alteration, Pd is more mobile than Pt, which in turn is much more mobile than IPGE and Rh (Wood, 2002; Hanley, 2005; Barnes and Liu, 2012). Additionally, base metal sulfides form secondary magnetite, pyrite, millerite and cubanite (Djon and Barnes, 2012; Pina et al., 2013; Holwell et al., 2017). Thus, hydrothermal alteration can produce anhedral Pt-Pd-PGM in sulfide fractures or enclosed in secondary sulfide and oxide minerals (Tao et al., 2007; Wang et al., 2008; Prichard et al., 2013b; Junge et al., 2019; Mansur et al., 2021) or result in Pd-depletion in sulfide ores (Liu et al., 2016; Li and Mungall, 2022).

In the Yangliuping and Zhengziyanwo deposits, the peridotite that hosts the disseminated and net-textured ores was completely altered into serpentine (Song et al., 2003). Serpentine, chlorite and anhedral magnetite grains were found in or around altered chalcopyrite or pyrrhotite grains in disseminated and net-textured ores (Figs. 2A, D). However, these sulfide ores show an overall increase of Ni, PGE to Cu without Pd or Pt anomalies in primitive-mantle normalized patterns (Figs. 3A-B). On the other hand, secondary magnetite, pyrite and millerite were not found in massive ores (Figs. 2C, F), breccia ores and Cu-rich ores (Figs. S1B-C) of the two deposits. Pd-PGM and $PtAs_2$ crystals found in the massive ores and Cu-rich ores were predominantly fully enclosed in BMS and CGSS crystals (Figs. 9C, E; Table 4). Thus, we conclude that hydrothermal alteration had only limited effect on whole-rock PGE contents of sulfide ores and the distribution of PGE in BMS in massive ores and Cu-rich ores from the Yangliuping and Zhengziyanwo deposits at the scale of whole-rock sample.

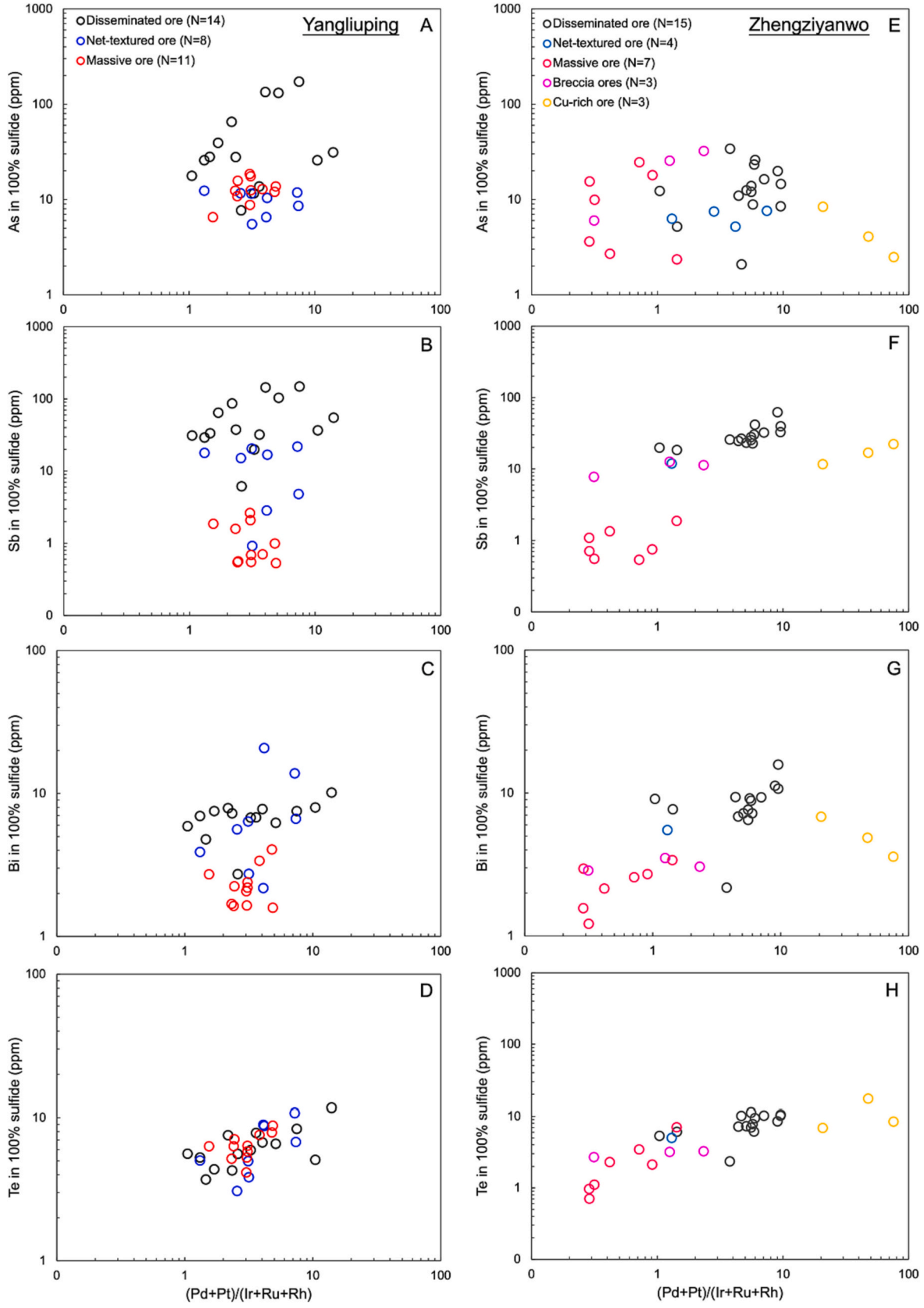

Fig. 5. Binary plots of whole-rock semimetals (in 100% sulfide) versus (Pt + Pd)/(Ir + Ru + Rh) for sulfide ores from the Yangliuping (A-D) and Zhengziyanwo (E-H) deposits. Whole-rock data are shown in Table S1.

Table 2
Number and type of PGE-peaks in the time-resolved spectra of LA-ICP-MS.

Deposit	Ore type	Sulfide	Pt-bearing	Pt-free
Yangliuping	Massive ore	Pyrrhotite	12	1
		Pentlandite	11	3
		Chalcopyrite	4	
		Total	27	4
Zhengziyanwo	Massive ore	Pyrrhotite	2	11
		Pentlandite	2	10
		Chalcopyrite		2
		Total	4	23
	Cu-rich ore	Chalcopyrite		1
		Total		1

5.2. Metal compositions of the Yangliuping and Zhengziyanwo deposits

The Cu-Ni-PGE deposits in the Yangliuping area are comagmatic with the Dashibao Formation basalts, which contain approximately 1 ppb Ir, 15 ppb Pt, 22 ppb Pd and 200 ppm Ni (Song et al., 2003, 2008). Song et al. (2008) shows that the Cu-Ni-PGE deposits at the Yangliuping area is formed from a parental magma weakly depleted in PGE, which experienced an earlier removal of about 0.01% sulfide. This is supported by Cu/Pd ratios of the disseminated ores at Yangliuping (approximately 4300 to 22,000) and Zhengziyanwo (approximately 2500 to 21,000) (Table S1).

This study shows that the sulfide liquids at the Yangliuping and Zhengziyanwo deposits (represented approximately by the disseminated ores, which underwent negligible fractional crystallization at the scale

Table 3
Average concentrations of PGE and semimetals in base metal sulfides of the sulfide ores from the Yangliuping and Zhengziyanwo deposits acquired using LA-ICP-MS.

Deposit	Ore type	Mineral	n	^{59}Co	^{193}Ir	Ru	^{103}Rh	^{195}Pt	Pd	^{75}As	^{121}Sb	^{125}Te	^{209}Bi
				ppm	ppb	ppb	ppb	ppb	ppb	ppm	ppm	ppm	ppm
Yangliuping	Massive ore (4 samples)	Po	39	252	4	209	5	15	10	0.8	0.3	1.2	0.2
		Pn	36	13,499	6	240	5	18	5167	0.6	0.3	1.1	0.0
		Ccp	20	2	4	19	5	8	299	0.7	0.4	3.6	0.3
Zhengziyanwo	Massive ore (3 samples)	Po	23	513	75	791	32	9	10	0.8	0.4	1.0	0.6
		Pn	21	11,582	54	611	26	9	6916	0.7	0.4	1.3	0.2
		Ccp	10	533	4	45	5	8	199	0.4	2.4	1.3	1.8
	Cu-rich ore (2 samples)	Po	15	457	5	22	5	8	10	0.6	0.3	1.5	0.5
		Pn	12	10,867	4	123	5	11	3020	0.4	0.6	2.6	0.1
		Ccp	10	6	4	13	5	8	420	0.4	0.5	6.9	0.7

The primary data is shown in Table S3. Po = pyrrhotite, Pn = pentlandite, Ccp = chalcopyrite. n = the number of LA-ICP-MS analyses spots.

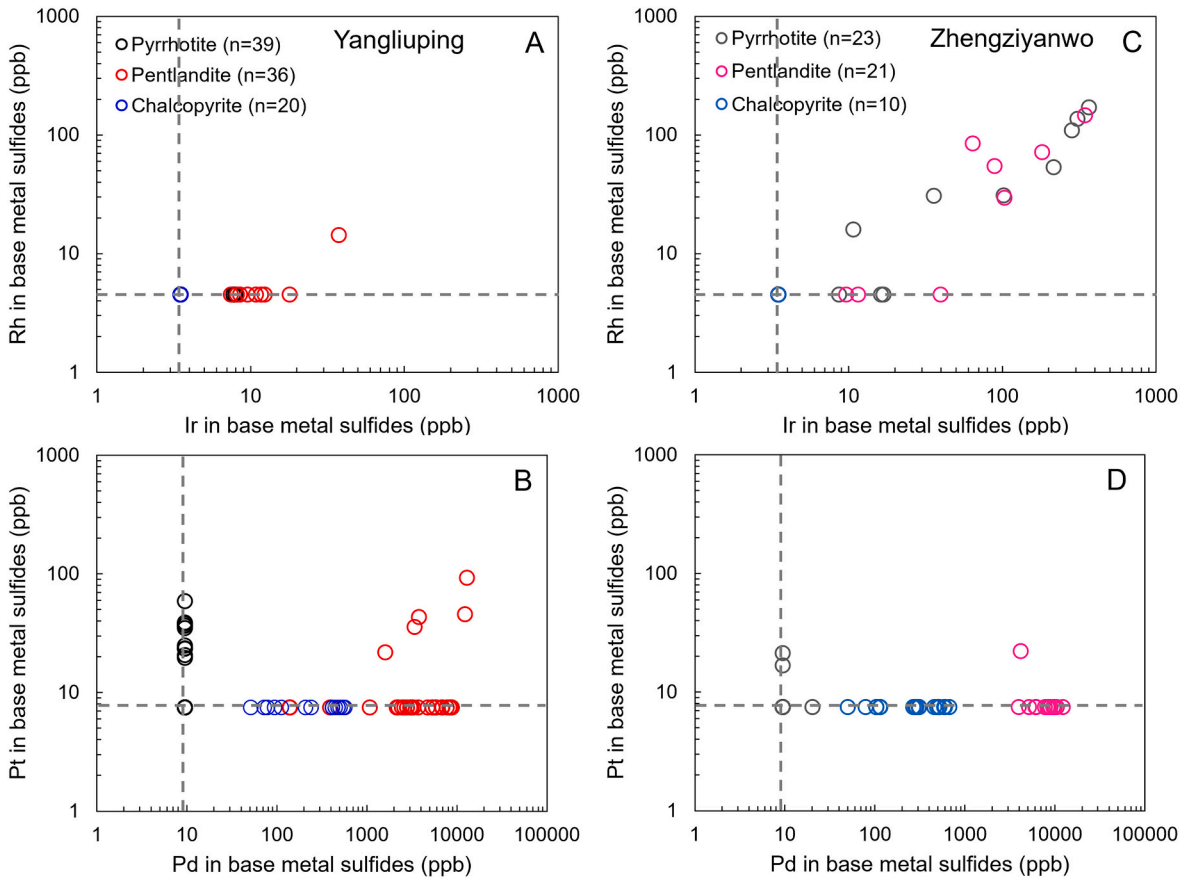

Fig. 6. Binary plots of Ir versus Rh and Pd versus Pt in the BMS of the Yangliuping massive ores (A-B) and the Zhengziyanwo massive ores (C-D). Dash grey lines indicate half detection limits for PGEs by LA-ICP-MS. The LA-ICP-MS data are given in Table S4 and spots with outliers were not plotted. Abbreviations: n = the number of LA-ICP-MS analyses spots.

Table 4
Number of PGM and CGSS found in sulfide ores from the Yangliuping and Zhengziyanwo deposits.

Deposit	Ore type	Locations	(Ir-Rh-Pt)AsS		$PtAs_2$	CGSS	PdTe	PdSbTe	PdBiTe
			(Ir-Rh-Pt)AsS	(Ir-Rh)AsS					
Yangliuping	Massive ore (4 samples)	Po	10	3	44	106		19	12
		Pn			8	8		1	
		Ccp	1		9	9			1
		CGSS	38	13	11				
		BMS-BMS			2	5		5	4
		Altered BMS			14	5			
		Total	65		88	133		25	17
Zhengziyanwo	Massive ore (3 samples)	Po				90	3	2	6
		Pn				17			
		Ccp				3			7
		CGSS	5	31					
		BMS-BMS				4			2
		Altered BMS		1		2			1
		Total	37			116	3	2	16
	Cu-rich ore (1 sample)	Po						6	
		Ccp			1				
		Total			1			6	

Note: (Ir-Rh-Pt)AsS = irarsite-hollingworthite-platarsite solid solution containing minor variable amount of Os and Ru, PtAs2 = sperrylite, CGSS = cobaltite-gersdorffite solid solution, PdTe = Kotulskite, PdBiTe = michenerite, PdSbTe = Testibiopalladite, Po = pyrrhotite, Pn = pentlandite, Ccp = chalcopyrite, BMS-BMS = pyrrhotite, pentlandite and chalcopyrite grain boundaries, altered BMS = secondary pyrite and magnetite.

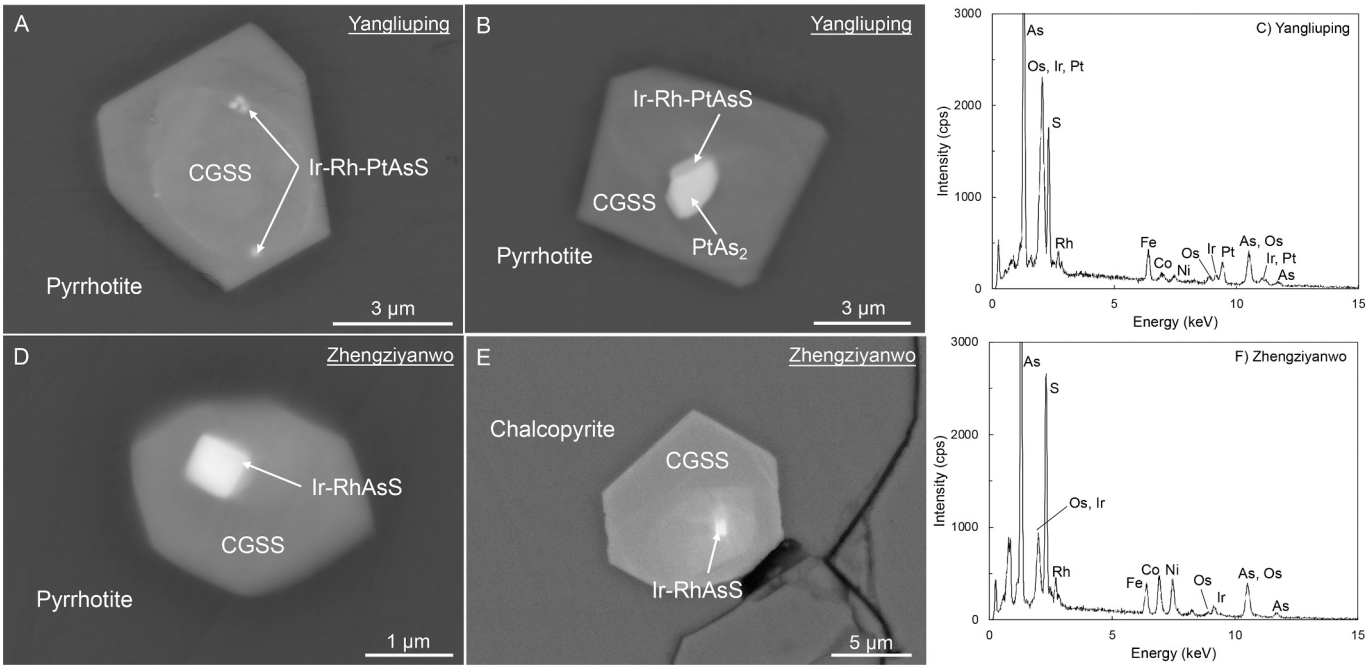

Fig. 7. Typical back scattered electron (BSE) images of the cobaltite-gersdorffite solid solution (CGSS) in Yangliuping massive ores (A-B) and Zhengziyanwo massive ores (D-E). Subhedral to euhedral (Ir-Rh-Pt)AsS and $PtAs_2$ particles were commonly found in the CGSS particles. Scanning Electron Microscopy energy dispersive X-ray spectra shows that Ir-Rh-PtAsS particles are enriched in Pt in Yangliuping massive ores (C) but poot in Pt in Zhengziyanwo massive ores (F). Abbreviation: CGSS = cobaltite-gersdorffite solid solution, Ir-Rh-PtAsS=Ir-Rh-(Pt) sulfarsenide, $PtAs_2$ = sperrylite.

of whole-rock sample) are distinctly different in chalcophile elements concentrations (Fig. 4A). This difference can be attributed to different degrees of earlier removal of sulfide from the parental magma (Song et al., 2008, 2009; Chen et al., 2013). As shown in sulfide segregation modelling (Fig. 11), the sulfide liquid at the Yangliuping deposit segregated from a parental magma with R-factors in the range of 300 to 3500, which experienced an earlier sulfide removal of about 0.006%. However, the sulfide liquid at the Zhengziyanwo deposit was segregated from a parental magma with R-factors varying from 1500 to 10,000, which underwent earlier sulfide removal of about 0.01%.

Magma saturated in sulfide at mantle sources may also exhibit PGE depletion (Keays, 1995; Arndt et al., 2005; Barnes et al., 2022). However, it is difficult to distinguish this from the PGE-undepleted magma that has undergone earlier sulfide liquid removal (Mungall and Brenan, 2014). Thus, the alternative is that the parent magma of the Yangliuping and Zhengziyanwo deposits was sulfide saturated at mantle sources with different proportions of sulfide retention.

5.3. The occurrence of PGE and formation of PGM in massive ores

The proportions of Co, PGE and semimetals occurring in BMS as solid solution were calculated following the method described by Barnes et al. (2008). The Ni content in the silicate portion of the samples was determined using the method proposed by Waal et al. (2004). The

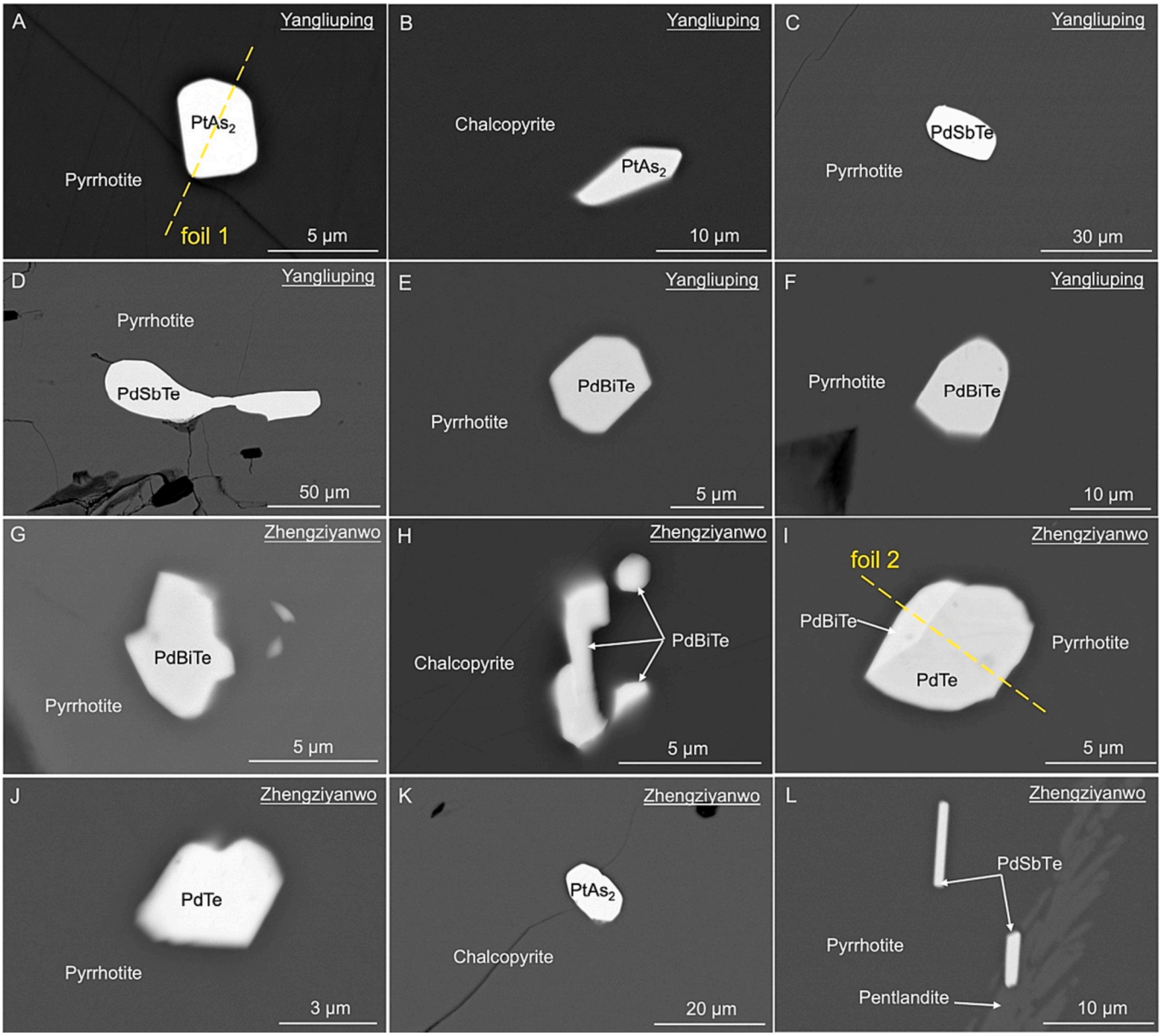

Fig. 8. Typical BSE images of PGMs in Yangliuping massive ores (A-F), Zhengziyanwo massive ores (G-J) and Zhengziyanwo Cu-rich ore (K-L). A-B. Euhedral to subhedral $PtAs_2$ enclosed in pyrrhotite and chalcopyrite crystals. C-D. Subhedral to anhedral PdSbTe particles enclosed in pyrrhotite crystals. E-F. Euhedral and subhedral PdBiTe particles enclosed in pyrrhotite crystals. G-H. Composite anhedral PdBiTe particles enclosed in pyrrhotite and chalcopyrite crystals. I. Composite grains of anhedral PdTe and PdBiTe particles enclosed in pyrrhotite crystal. J. Anhedral PdTe particle in pyrrhotite. K. Subhedral sperrylite enclosed in chalcopyrite from Cu-rich ores. L. PdSbTe particles with a lath shape enclosed in pyrrhotite and located at the phase boundaries between pyrrhotite and pentlandite from Cu-rich ores. Yellow dash lines annotated with foil numbers indicate the positions for focused iron beam (FIB) sample preparations. Abbreviation: $PtAs_2$ = sperrylite, PdSbTe = testibiopalladite, PdTe = kotulskite, PdBiTe = michenerite. (For interpretation of the references to colour in this figure legend, the reader is referred to the web version of this article.)

details can be found in Liang et al. (2022). In the Yangliuping massive ores, Zhengziyanwo massive ores and Cu-rich ores, <7% of Ir, Rh and Pt occur in BMS as solid solution (Fig. 12). Interestingly, the amount of Pd present in solid solution within BMS in the Yangliuping massive ores (17%) (Fig. 12A) is significantly lower than that in the Zhengziyanwo massive ores (91%) (Fig. 12B). The balance of PGE is accounted for by the nanometer-sized Ir-Rh-(Pt)AsS, micrometer-sized CGSS, $PtAs_2$ and Pd-PGM particles (Fig. 7, Fig. 8, Table 4).

Ir-Rh-(Pt)AsS, $PtAs_2$ and CGSS particles found in the Yangliuping and Zhengziyanwo massive ores mainly show euhedral shapes (Fig. 7, Figs. 8A-B, Fig. 9D). These particles are enclosed in pyrrhotite, pentlandite and chalcopyrite (Fig. 9C, Table 4) indicating early crystallization from sulfide liquids (Power et al., 2004; Dare et al., 2010b; Liang et al., 2019). No magmatic magnetite was found in the Yangliuping and Zhengziyanwo massive ores (Figs. 2C-D, E-F), which indicates that the sulfide liquids had relatively low fO_2 and high As^{n-}/As^{n+} ratio (Liang et al., 2022). As^{n-} forms Ir-AsS, Rh-AsS and Pt-As pre-nucleation clusters in sulfide liquids (Helmy et al., 2013; Helmy and Bragagni, 2017). These pre-nucleation clusters were enriched near the migrating MSS and CGSS grain boundaries, leading to oversaturation and nucleation of Ir-Rh-(Pt)AsS and $PtAs_2$ crystals (Liang et al., 2022). These PGM particles were either overgrown by CGSS, MSS, and ISS or served as nucleation sites for later-crystallized CGSS. As a result, they were found in the core and brighter zones of CGSS (Figs. 7A-B, D-E) and within BMS crystals (Figs. 8A-B, Table 4) (Dare et al., 2010b; Liang et al., 2019). This process is supported by the microstructure of $PtAs_2$ which shows no preferred

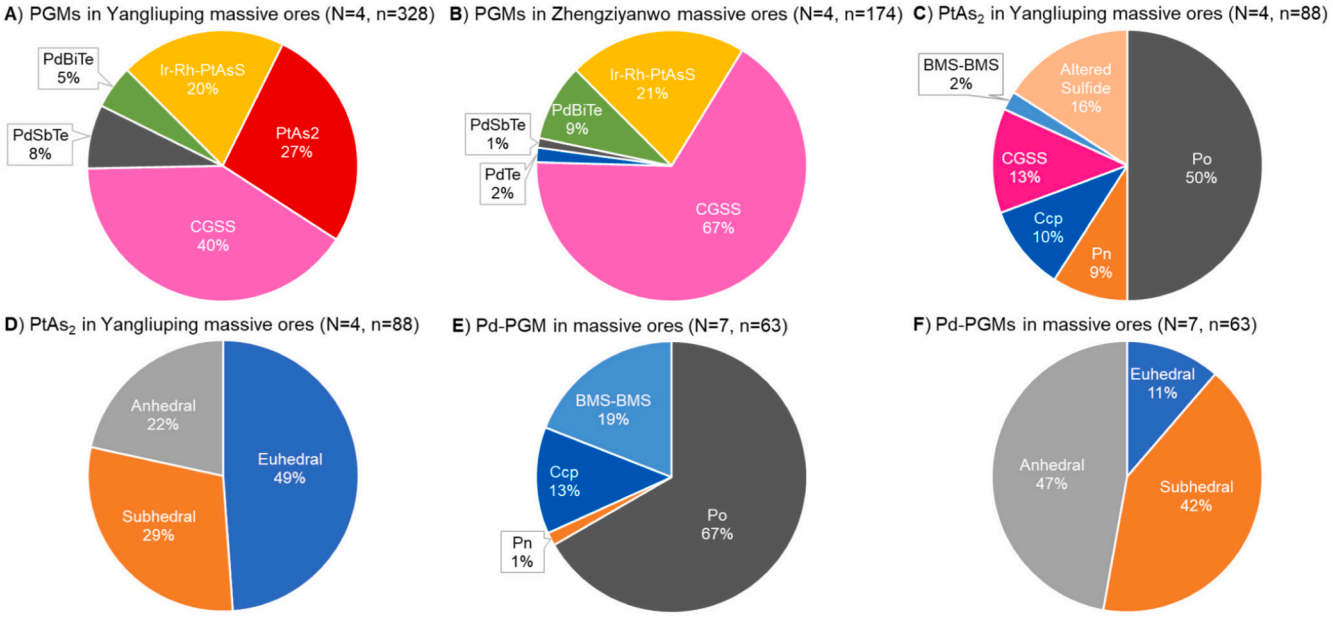

Fig. 9. Pie diagrams showing relative proportions (%) and morphology of PGM in sulfide ores at the Yangliuping and Zhengziyanwo deposits. A-B. The proportions of different types of PGM in Yangliuping massive ores (A) and Zhengziyanwo massive ores (B). C-D. The locations (C) and morphology (D) of $PtAs_2$ particles in the Yangliuping massive ores. E-F. The locations (E) and morphology (F) of Pd-PGMs (PdTe, PdSbTe and PdBiTe) in the Yangliuping and Zhengziyanwo massive ores. The proportion of each kind of mineral is given in number and the source data are shown in Table 3. Abbreviation: Ir-Rh-PtAsS=Ir-Rh-(Pt) sulfarsenide, $PtAs_2$ = sperrylite, PdSbTe = testibiopalladite, PdTe = kotulskite, PdBiTe = michenerite.

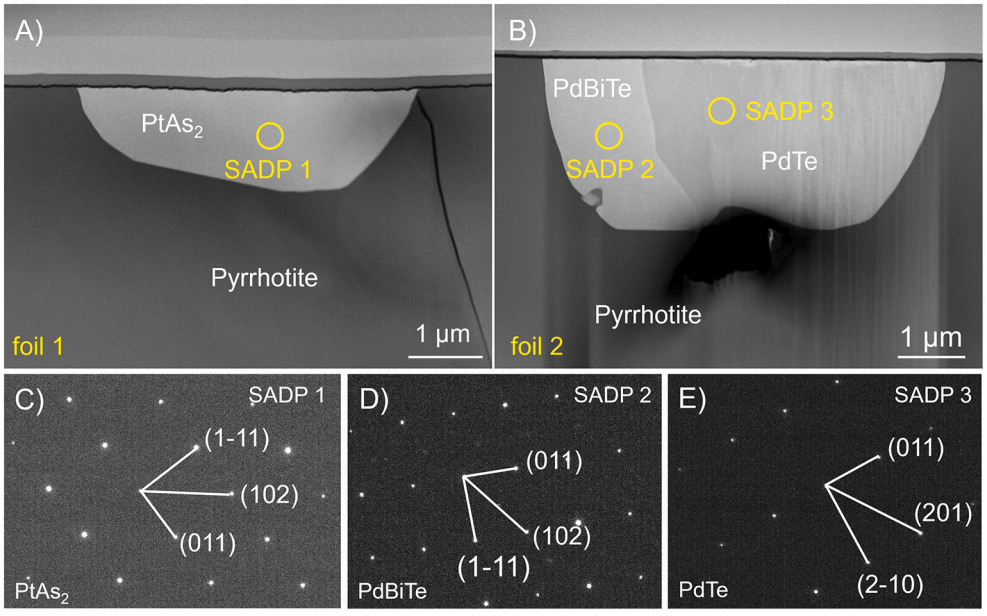

Fig. 10. Typical high-angle annular dark field (HAADF) images and selected-area diffraction pattern of typical platinum-group minerals. The foil numbers are corresponding to the numbers in annotated in Fig. 6. A. $PtAs_2$ enclosed in pyrrhotite from Yangliuping massive ore. B. composite grains of PdTe and PdBiTe enclosed in pyrrhotite from Zhengziyanwo massive ore. The black hole below the platinum-group minerals in Fig. 8B was produced during foil preparation. The chemical composition and selected area diffraction patterns (SADP) acquired using transmission electron microscopy (TEM) confirmed that these PGM are $PtAs_2$ (Fig. 8A, C), PdBiTe and PdTe (Fig. 8B, D-E), respectively. Abbreviation: $PtAs_2$ = sperrylite, PdTe = kotulskite, PdBiTe = michenerite.

orientation relationship with the host pyrrhotite crystal (Fig. 10A). $PtAs_2$, (Ir-Rh-Pt)AsS and CGSS crystallized early from sulfide liquids were also recognized in the Jinchuan deposit (Prichard et al., 2013b; Liang et al., 2022), the Creighton deposit, Sudbury (Dare et al., 2010a, 2010b), the Main Sulfide Zone of Great Dyke (Coghill and Wilson, 1993), the Platreef and Merensky Reef, Bushveld Complex (Junge et al., 2014) and in the ultramafic intrusion at Lavatrafo, Madagascar (Ohnenstetter et al., 1999; McDonald, 2008).

Stoichiometric PdBiTe, PdSbTe and PdTe crystallizes in sulfide liquids at relatively low temperatures (525 °C to 740 °C) (Makovicky, 2002 and references therein). In the Yangliuping and Zhengziyanwo massive ores, the micrometer-sized Pd-PGM particles mainly occur within pyrrhotite (Fig. 9E) as individual grains or composite grains (Figs. 8C-J). The PdTe and PdBiTe particles within pyrrhotite show anhedral to subhedral shapes in TEM HAADF images (Fig. 10B) and show no preferred orientation relationship with the host pyrrhotite. These particles crystallized near migrating grain boundaries of MSS (Distler et al., 2016; Liang et al., 2022) or from Pd-semimetals-rich droplets enclosed in MSS (Cabri and Laflamme, 1976; Helmy et al., 2020, 2023), rather than forming by exsolution, which would have resulted in oriented

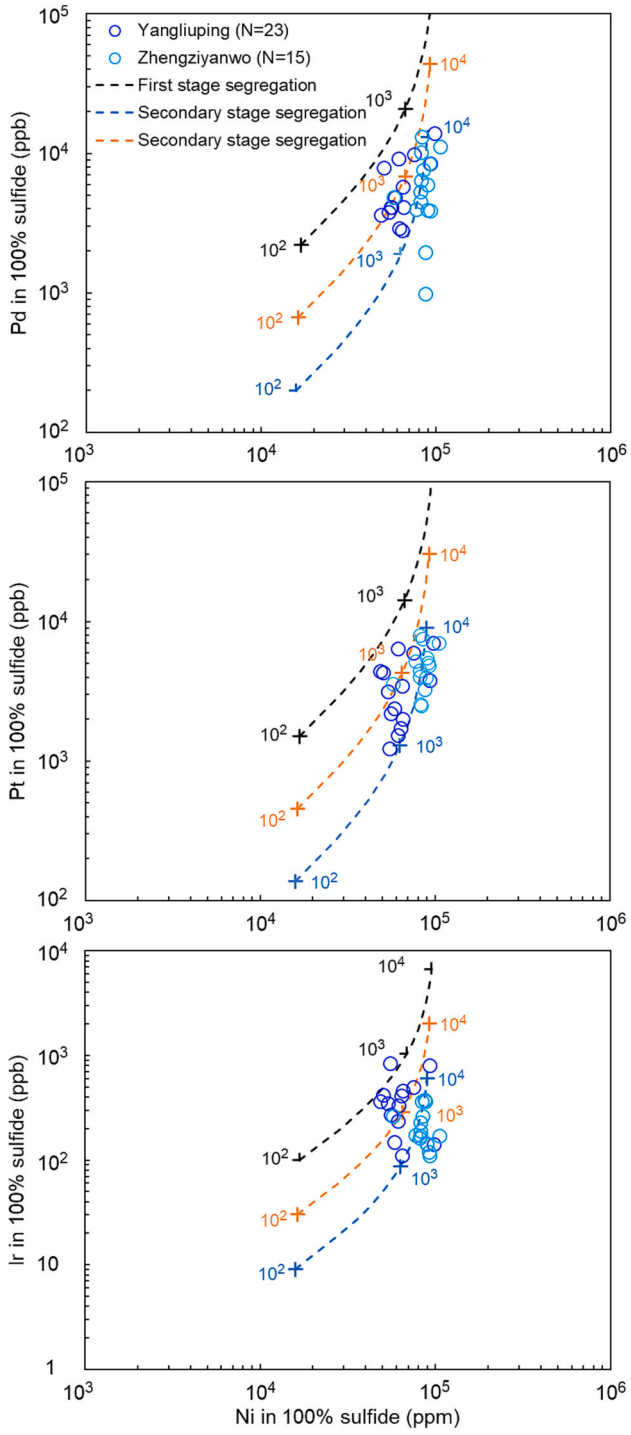

Fig. 11. Modelling of Ni and PGE concentrations (in 100% sulfides) in disseminated ores from the Yangliuping and Zhengziyanwo deposits. The first stage segregation (black dash line) represents the sulfide liquids segregated from PGE undepleted magma containing 1 ppb Ir, 15 ppb Pt, 22 ppb Pd, 200 ppm Ni (Song et al., 2008) under various R factors (annotated as crosses with numbers). Secondary stage segregations (orange and blue dash lines) represent sulfide liquids segregated from PGE depleted magma. Orange dash line indicates sulfide liquid segregated from PGE depleted magma containing 0.3 ppb Ir, 6.63 ppb Pd, 4.52 ppb Pt and 194 ppm Ni (after 0.006% sulfide removal). Blue dash line represents sulfide liquids segregated from PGE depleted magma containing 0.09 ppb Ir, 2 ppb Pd, 1.36 ppb Pt and 188 ppm Ni (after about 0.01 sulfide removal). $D_{Ni}^{Sul/Sil} = 500$ and $D_{Ir,\ Pd,\ Pt}^{Sul/Sil} = 20{,}000$ (Li and Audétat, 2012; Mungall and Brenan, 2014; Zhang and Li, 2021) were used in the modelling. (For interpretation of the references to colour in this figure legend, the reader is referred to the web version of this article.)

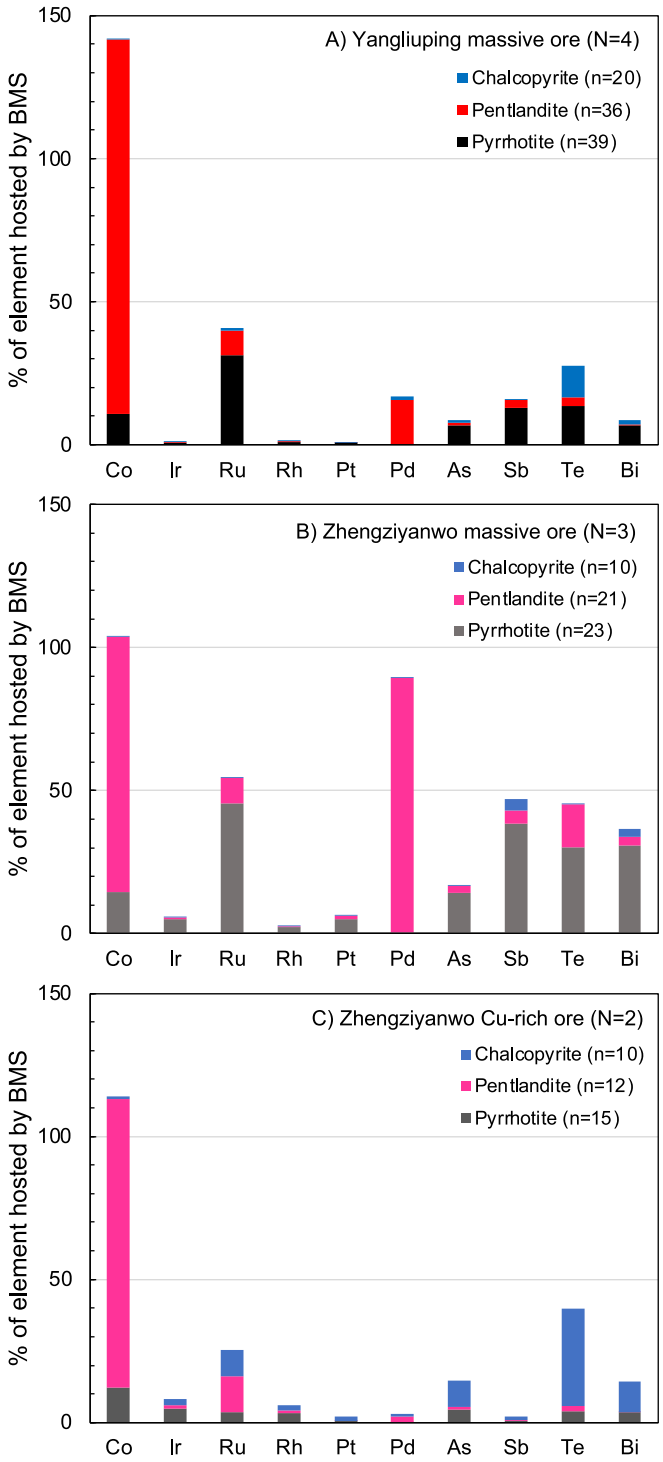

Fig. 12. Mass balance of the Co, PGE and semimetals in BMS of Yangliuping massive ores (A), Zhengziyanwo massive ores (B) and Cu-rich ores (C). Each graph is plotted as the proportion of each element in pyrrhotite, pentlandite and chalcopyrite. The original data are shown in Table S5. Abbreviations: N = the number of sulfide ores analyzed, n = the number of LA-ICP-MS analyses spots.

lamellae within host minerals (Putnis, 1992; Wirth et al., 2013). However, we cannot completely rule out the possibility that the lath-shaped PdSbTe particles (Fig. 8L) formed by exsolution during cooling (Makovicky et al., 1986; Ballhaus and Ulmer, 1995; Barnes et al., 2008).

5.4. The effect of PGM particles on PGE differentiation

5.4.1. Incorporation of Pd-PGM and $PtAs_2$ particles resulted in Pt-Pd-enrichment in Yangliuping massive ores

The sulfide liquid at the Yangliuping deposit had comparable Pd and lower Pt concentrations compared to that at the Zhengziyanwo deposit (Fig. 4A). However, Yangliuping massive ores have higher Pd and Pt tenors (about 4 ppm Pd and 2 ppm Pt on average) than Zhengziyanwo massive ores (about 1 ppm Pd and 0.5 ppm Pt on average) (Figs. 3C-D, Table 1). In the Ni/(Ru × 1000) versus Pd/Ru diagram of fractional crystallization modelling (Fig. 13C), Zhengziyanwo massive ores plot on the MSS cumulate trend, which indicates that the differentiation of Pd among different types of sulfide ores is mainly controlled by the partition coefficient and Pd-Cu-rich residual sulfide liquids have migrated away thus forming Pd-Cu-rich ores (Fig. 3D). This is consistent with the relatively high proportion of Pd (91%) occurring in BMS as solid solution (Fig. 12B) (Mansur et al., 2019b). As for the Yangliuping deposit, the massive ores have comparable Pd and Pt tenors with the disseminated ores and net-textured ores (Fig. 3C), and they plot on the residual liquid trend in the fractional crystallization modelling diagram (Figs. 13A-B). This indicates that the Yangliuping massive ores have higher Pd and Pt contents than that predicted by chemical equilibrium partition modelling.

Pd in residual sulfide liquids can diffuse into high temperature pentlandite formed by peritectic reaction (Mansur et al., 2019a; Barnes et al., 2020). The average concentration of Pd in pentlandite of the Yangliuping massive ores (approximately 5 ppm) is lower than that of the Zhengziyanwo massive ores (approximately 7 ppm) (Table 3). Furthermore, about 83% Pd in the Yangliuping massive ores occurs as Pd-PGM (Fig. 12A), which were mainly enclosed in pyrrhotite crystals (Fig. 9E). Therefore, Pd having diffused into pentlandite is not the mechanism resulting in the enrichment of Pd in the Yangliuping massive ores.

As discussed above, the majority of Pt and Pd in the Yangliuping massive ores occur as $PtAs_2$ and Pd-PGM (all are Pd-tellurides, Table 4) (Fig. 12A), which crystallized near the migrating grain boundaries of MSS or from Pd-(Pt)-semimetals-rich droplets (Cabri and Laflamme, 1976; Sinyakova and Kosyakov, 2012; Liang et al., 2022). We propose that the incorporation of the PGM particles or Pd-(Pt)-semimetals-rich droplets into cumulated MSS crystals, or their trapping in MSS intercumulus spaces, resulted in the enrichment of Pd and Pt in the Yangliuping massive ores (Fig. 3C). These PGM particles finally occur as

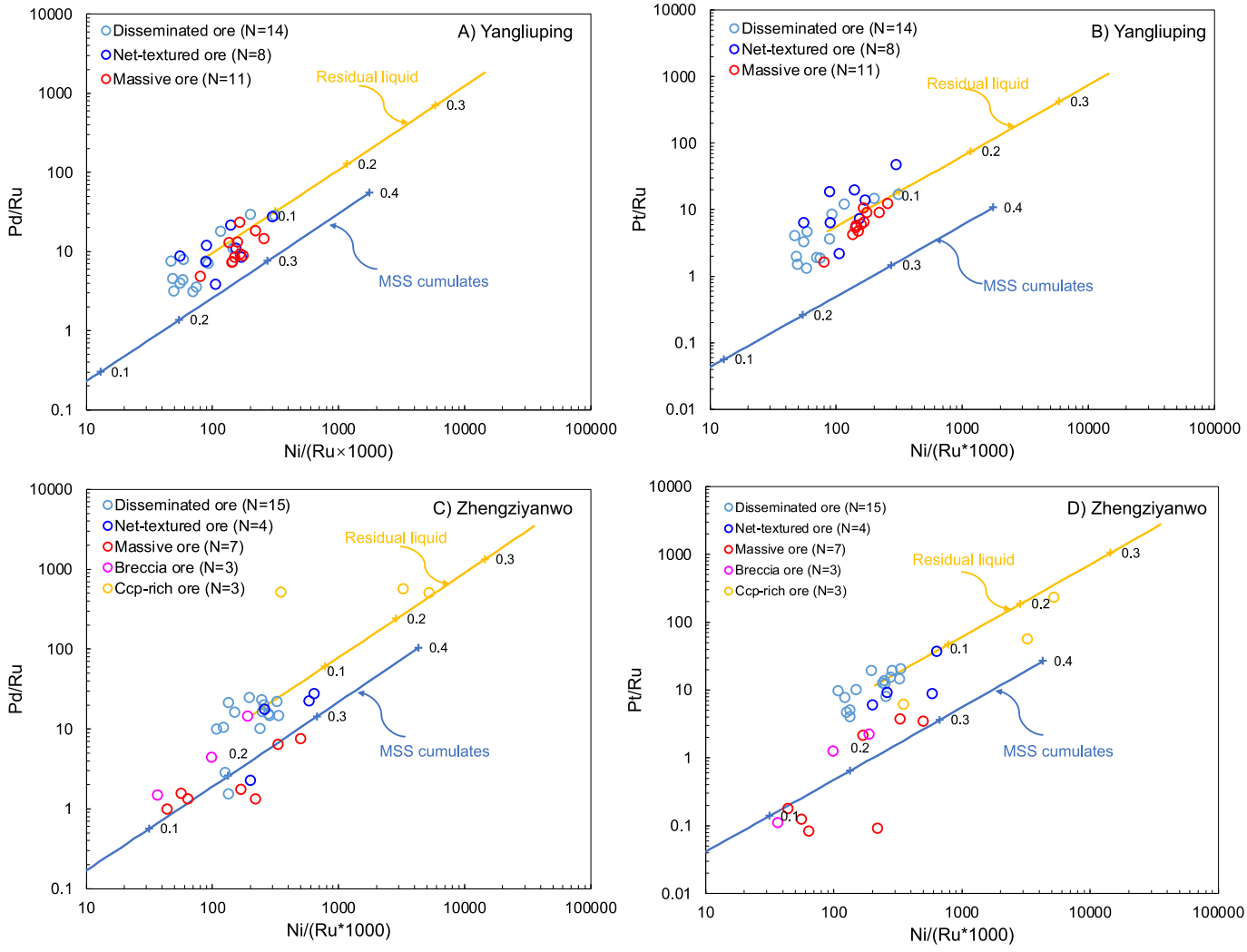

Fig. 13. Fractionation crystallization modelling for the sulfide liquids from the Yangliuping deposit (A-B) and the Zhengziyanwo deposit (C-D). Whole-rock data are listed in Table S1. MSS cumulates and residual liquid trends were calculated using a Rayleigh equation. Crosses annotated with numbers represent the degrees of fractionation. According to average composition of disseminated ores, the sulfide liquid of the Yangliuping deposit was assumed to contain 6.46 wt% Ni, 854 ppb Ru, 6143 ppb Pd and 3548 ppb Pt, whereas the sulfide liquid of the Zhengziyanwo deposit was assumed to contain 8.49 wt% Ni, 454 ppb Ru, 6204 ppb Pd and 4725 ppb Pt. $D_{Pd}^{MSS/Sul} = 0.133$, $D_{Ru}^{MSS/Sul} = 13$ and $D_{Pt}^{MSS/Sul} = 0.045$ (Li et al., 1996; Liu and Brenan, 2015; Mungall and Brenan, 2014) were used in the modelling. $D_{Ni}^{MSS/Sul}$ is assumed to be 0.6 at the beginning and increases gradually to 0.9 after ~50% of the sulfide liquid has solidified (Mungall et al., 2005)

individual or composite grains within pyrrhotite and pentlandite or located at BMS grain boundaries (Figs. 8A-F). As a result, in the Yangliuping massive ores, more $PtAs_2$ and Pd-PGM particles were found (Fig. 9A) and a lower proportion of Pd occur in BMS as solid solution (Fig. 12A) compared to the Zhengziyanwo massive ores (Fig. 9B, Fig. 12B). This process also enriched the Yangliuping massive ores with As and Te (Figs. 5A, D) but not with Sb and Bi (Figs. 5B-C).

5.4.2. *Early fractional crystallization of $PtAs_2$ in sulfide liquids at the Zhengziyanwo deposit*

Several interpretations have been proposed to explain the negative Pt anomalies of massive ores in Cu-Ni-PGE deposits. These include early fractional crystallization of Pt-PGM (Song et al., 2009; Chen et al., 2013; Smith et al., 2022), nugget effects (Savard et al., 2010; Barnes et al., 2022), migration of Pt-Cu-rich residual sulfide liquids (Chen et al., 2013) and post-magmatic hydrothermal processes (Su et al., 2008).

Nugget effects have been observed in whole-rock analyses of natural samples (Savard et al., 2010; Barnes et al., 2022). Barnes et al. (2022) suggested that the presence of sparse Pt-rich grains may result in greater variability of Pt compared to other PGE in subsamples. In our study, $PtAs_2$ particles were found in the Yangliuping massive ores (Fig. 9A) but not in the Zhengziyanwo massive ores (Fig. 9B). Despite this, no Pt anomaly was observed in the Yangliuping massive ores (Fig. 3C), while the Zhengziyanwo massive ores and breccia ores exhibited negative Pt anomalies (Fig. 3D). On the other hand, the CRMs analyzed in this study show good consistency with their certified values, and both the replicated samples and CRMs show good reproducibility (Fig. 14), although Ir, Rh and Pt mainly occurred as PGM in the Yangliuping and Zhengziyanwo massive ores (Figs. 12A-B). These results suggest that the method for whole-rock PGE analyses (Qi et al., 2011) used in this study is capable of resolving $PtAs_2$ particles. Therefore, nugget effects are not the cause of Pt depletion in the Zhengziyanwo massive ores and breccia ores.

As previously mentioned, hydrothermal alteration had limited effect on massive ores, breccia ores and Cu-rich ores. In the Zhengziyanwo deposit, both the massive ores and breccia ores exhibit negative Pt anomalies, while the Cu-rich ores are not enriched in Pt compared to the disseminated ores and net-textured ores (Fig. 3D). These observations indicate that the depletion of Pt in the Zhengziyanwo massive ores was not caused by hydrothermal alteration or the migration of Pt-Cu-rich residual sulfide liquids.

In the Yangliuping and Zhengziyanwo deposits, only $PtAs_2$ and Ir-Rh-(Pt)AsS have been found as Pt-bearing PGM (Figs. 9A-B, Table 4) (Song et al., 2004 and references therein; Liang et al., 2019). The sulfide liquid at the Zhengziyanwo deposit has a higher Pt concentration compared to that at the Yangliuping deposit (Fig. 4A). In contrast, micrometer-sized $PtAs_2$ and nanometer-sized Ir-Rh-(Pt)AsS particles are common in the Yangliuping massive ores (Fig. 9A, Table 4), whereas no $PtAs_2$ particles were found and Ir-Rh-(Pt)AsS particles have low Pt content in the Zhengziyanwo massive ores (Fig. 9B, Table 4). Experimental studies have shown that IrAsS and RhAsS begin to crystallize at temperatures >1200 °C in sulfide liquids (Helmy and Bragagni, 2017), whereas $PtAs_2$ can form at temperature up to 1400 °C (Hansen et al., 1958; Bennett and Heyding, 1966). This suggests that $PtAs_2$ can crystallize earlier than Ir-Rh-(Pt)AsS in sulfide liquids, as evidenced by zoned PGM with $PtAs_2$ cores and Ir-Rh-(Pt)AsS rims within CGSS crystals from the Sudbury-Creighton deposit (Fig. 7I in Dare et al., 2010a). We conclude that the early fractional crystallization of $PtAs_2$, likely accompanied by MSS, resulted in the depletion of Pt in the sulfide liquid at the Zhengziyanwo deposit, which leads to the formation of low-Pt Ir-Rh-(Pt)AsS particles and Pt-depleted massive ores, breccia ores, and Cu-rich ores. This process enriched the Zhengziyanwo Cu-rich ores with Sb, Bi and Te (Figs. 5F-H) but not with As (Fig. 5E) compared to the massive ores.

The assimilation of country rocks increases semimetal concentrations, leading to the crystallization of PGM (Hutchinson and Kinnaird, 2005; Holwell et al., 2006; Hutchinson and McDonald, 2008; Dare et al., 2010b, 2011; Yudovskaya et al., 2017). The sulfide liquid at the Zhengziyanwo deposit has a lower As concentration than that at the Yangliuping deposit (Fig. 4B). The early crystallization of $PtAs_2$ in the Zhengziyanwo deposit can be attributed to differences in thermodynamic conditions (fS_2 and fO_2) of the sulfide liquids. The valence states of As in sulfide liquids are variable and controlled by thermodynamic conditions (Helmy et al., 2010; Helmy and Bragagni, 2017). In Cu-Ni-PGE deposits, fO_2 mainly controls the valence state of As in sulfide liquids (Liang et al., 2022). The sulfide liquid at the Zhengziyanwo deposit has a relatively higher fS_2 (Fig. 15) thus a relatively lower fO_2 compared to the sulfide liquid at the Yangliuping deposit (Liang et al., 2022). As a

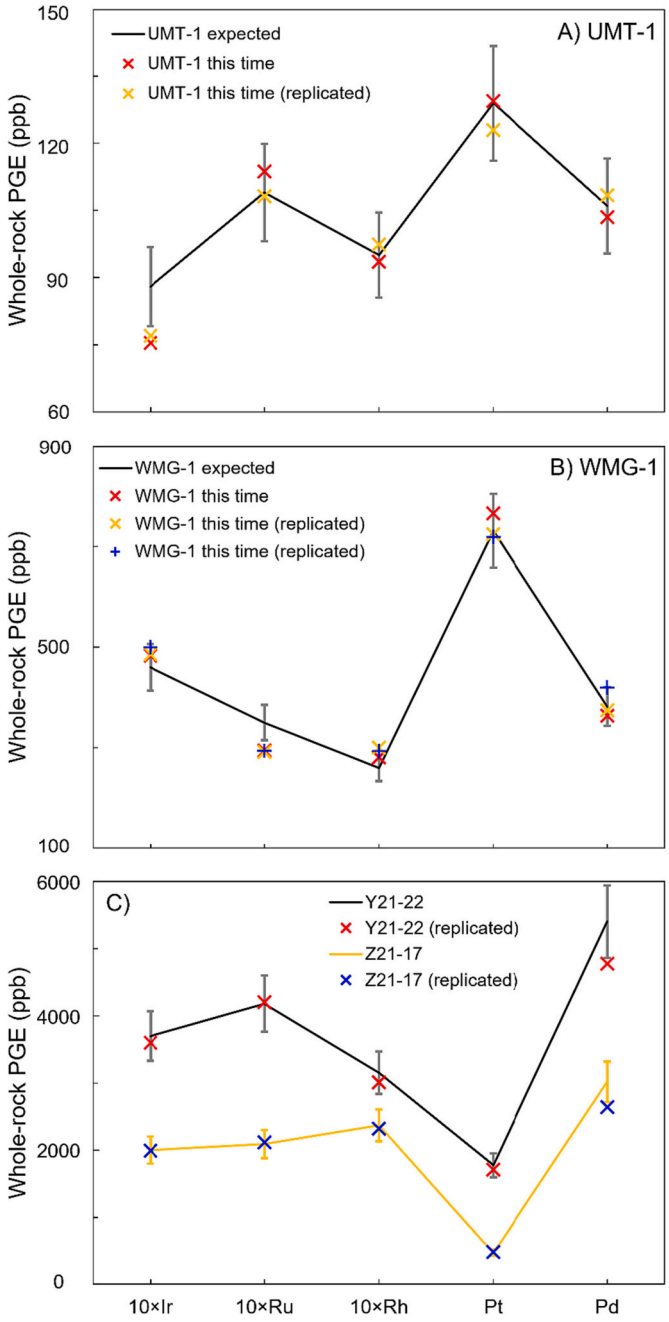

Fig. 14. Whole-rock platinum-group elements analyses of UMT-1 (A), WMG-1 (B) and two samples from the Yangliuping and Zhengziyanwo deposits (C). Ir, Ru and Rh concentrations are multiplied by 10 to show concentration variations more clearly. Error bars indicates 10% relative errors of the expected PGE concentrations (UMT-1 and WMG-1) and measured PGE concentrations (Y21–22 and Z21–17). The data are shown in Table S2.

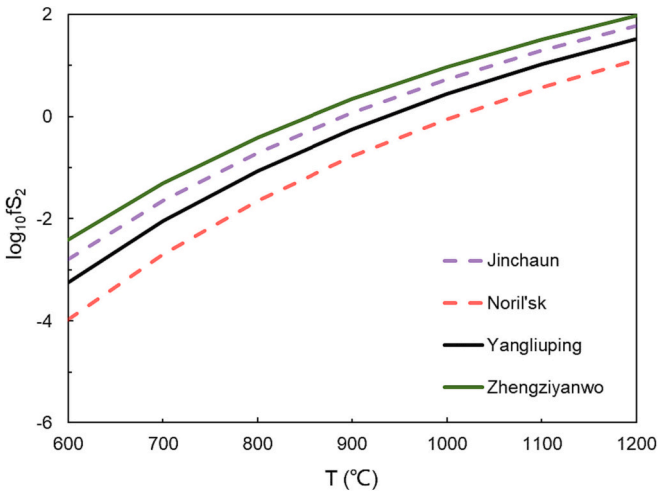

Fig. 15. Equilibrium temperature-dependent variations of sulfur fugacity of sulfide liquids from the Yangliuping and Zhengziyanwo deposits. The sulfur fugacity was calculated based on the average compositions of pyrrhotite in massive ores (Table S6) using the equation Mengason et al. (2010) modified from Toulmin and Barton (1964). The pyrrhotite in massive ores were assumed to be in equilibrium with the sulfide liquids during crystallization. The sulfide liquids of the two deposits were assumed to be closed systems according to the absence of magmatic magnetite at the sulfide-silicate boundaries (Fonseca et al., 2008). The data for Jinchuan and Noril'sk are from Liang et al. (2022).

result, it is likely that the As^{n-}/As^{n+} ratio in Zhengziyanwo sulfide liquid is higher, leading to the formation of more Pt-As pre-nucleation clusters. This indicates that the saturation of $PtAs_2$ can be achieved earlier in the sulfide liquid at Zhengziyanwo than that at Yangliuping.

5.5. Implications

Recent studies have shown that euhedral IrAsS, RhAsS and $PtAs_2$ particles can crystallize from natural sulfide liquids (Coghill and Wilson, 1993; Ohnenstetter et al., 1999; Power et al., 2004; Mcdonald, 2008; Dare et al., 2010b; Prichard et al., 2013b; Liang et al., 2019, 2022). This study indicates that $PtAs_2$ crystals crystallized earlier in the Zhengziyanwo deposit due to the relatively lower fO_2 of the sulfide liquid compared to the Yangliuping deposit. This provides additional evidence supporting the model that the fO_2 affect the valence state of As thus controls the behavior of Pt in sulfide liquids of Cu-Ni-PGE deposits (Liang et al., 2022).

On the other hand, PGM particles or PGE-clusters have been proposed to play an important role in PGE enrichment in sulfide liquids and mafic-ultramafic intrusions (Tredoux et al., 1995; McDonald, 2008; Wirth et al., 2013; Junge et al., 2014; Maier et al., 2015; González-Jiménez et al., 2018; Kamenetsky and Zelenski, 2020), in PGE differentiation during partial melting of the Earth's mantle (Ballhaus et al., 2006; González-Jiménez et al., 2019) and during solidification of sulfide liquids in magmatic Cu-Ni-PGE deposits (Song et al., 2009; Chen et al., 2013; Liang et al., 2019, 2022; Smith et al., 2022). Our study confirms that the fractional crystallization of $PtAs_2$ and Pd-PGM particles and their incorporation into MSS cumulates are crucial in forming the Pt-depleted sulfide ores at the Zhengziyanwo deposit and the Pd-Pt-rich massive ores at the Yangliuping deposit. Accordingly, the role of PGM particles should be considered when using PGE to trace the fractional crystallization of sulfide liquids in Cu-Ni-PGE deposits. Meanwhile, this study also suggests a potential for exploring Pt-rich sulfide ores in the Zhengziyanwo deposit.

6. Conclusion

The sulfide liquid at the Yangliuping deposit has similar Pd but lower Pt concentrations compared to the Zhengziyanwo deposit. In both deposits, massive ores were formed by the cumulation of MSS, and hydrothermal alteration had limited effects on the concentration and distribution of PGE in massive ores, breccia ores and Cu-rich ores at the scale of whole-rock sample. In the Yangliuping deposit, the massive ores are enriched in Pd and Pt showing similar PGE concentrations to disseminated ores and net-textured ores. In contrast, the massive ores and breccia ores in the Zhengziyanwo deposit are all depleted in Pt. In the massive ores from both deposits, >93% of Ir, Rh, and Pt occur as Ir-Rh-(Pt)AsS and $PtAs_2$. In the Yangliuping and Zhengziyanwo massive ores, 83% and 11% of Pd occur as Pd-PGM, respectively. The Ir-Rh-(Pt)AsS, $PtAs_2$ and Pd-PGM particles in the massive ores occur as individual or composite grains and were mainly found enclosed in pyrrhotite, pentlandite, chalcopyrite and CGSS crystals. These PGM crystallized from the sulfide liquids or from Pd-semimetals-rich droplets.

The incorporation of Pd-PGM and $PtAs_2$ particles into cumulated MSS or their trapping in intercumulus spaces resulted in the enrichment of Pd and Pt in the massive ores at the Yangliuping deposit. In contrast, in the Zhengziyanwo deposit, the early fractional crystallization of $PtAs_2$ formed Pt-depleted sulfide liquids, from which Pt-depleted massive ores, breccia ores and Cu-rich ores formed, and low-Pt Ir-Rh-(Pt)AsS particles crystallized. This study provides further evidence supporting the model proposed by Liang et al. (2022) that Pt forms Pt-As pre-nucleation clusters prompting the early crystallization of $PtAs_2$ in natural sulfide liquids with relatively low fO_2. Additionally, this study shows that PGM play a significant role in the enrichment and differentiation of PGE in magmatic Cu-Ni-PGE deposits. We propose that there is a potential for exploring Pt-rich sulfide ores in the Zhengziyanwo deposit.

Declaration of Competing Interest

The authors declare that they have no known competing financial interests or personal relationships that could have appeared to influence the work reported in this paper.

Data availability

Data will be made available on request.

Acknowledgement

This work was financially supported by grants from the National Natural Science Foundation of China (42121003, 41772067 and 41630316). We are grateful to Yi Fang for assistance with sample collection, Yuan-Yun Wen for in foil preparation and Jia-Ni Chen for help in TEM analyses. We also acknowledge Iain McDonald and one anonymous reviewer for their detailed reviews and constructive comments. We thank Editor Marco Fiorentini and Associate Editor Dhilip Kumar for their efficient handing of our manuscript.

Appendix A. Supplementary data

Supplementary data to this article can be found online at https://doi.org/10.1016/j.chemgeo.2023.121645.

References

Anenburg, M., Mavrogenes, J.A., 2016. Experimental observations on noble metal nanonuggets and Fe-Ti oxides, and the transport of platinum group elements in silicate melts. Geochim. Cosmochim. Acta 192, 258–278.
Anenburg, M., Mavrogenes, J.A., 2020. Noble metal nanonugget insolubility in geological sulfide liquids. Geology 48, 939–943.
Arndt, N.T., Lesher, C.M., Czamanske, G.K., Arndt, N.T., Lesher, C.M., Czamanske, G.K., 2005. Mantle-derived magmas and magmatic Ni-Cu-(PGE) deposits. Econ. Geol. 5–24.
Ballhaus, C., Sylvester, P., 2000. Noble metal enrichment processes in the Merensky Reef, Bushveld Complex. J. Petrol. 41 (4), 545–561.

Ballhaus, C., Ulmer, P., 1995. Platinum-group elements in the Merensky Reef: II. Experimental solubilities of platinum and palladium in $Fe_{1-x}S$ from 950 to 450°C under controlled f_{S2} and f_{H2}. Geochim. Cosmochim. Acta 59, 4881–4888.
Ballhaus, C., Bockrath, C., Wohlgemuth-Ueberwasser, C., Laurenz, V., Berndt, J., 2006. Fractionation of the noble metals by physical processes. Contrib. Mineral. Petrol. 152, 667–684.
Barnes, S.J., 2004. Komatiites and nickel sulfide ores of the Black swan area, Yilgarn Craton, Western Australia. 4. Platinum group element distribution in the ores, and genetic implications. Mineral. Deposita 39 (7), 752–765.
Barnes, S.J., Lightfoot, P.C., 2005. Formation of magmatic nickel sulfide ore deposits and processes affecting their copper and platinum group element contents. Econ. Geol. 100, 179–213.
Barnes, S.J., Liu, W.H., 2012. Pt and Pd mobility in hydrothermal fluids: evidence from komatiites and from thermodynamic modelling. Ore Geol. Rev. 44, 49–58.
Barnes, S.J., Maier, W.D., 1999. The fractionation of Ni, Cu and the noble metals in silicate and sulphide liquids. In: Keays, R.R., Lesher, C.M., Lightfoot, P.C., Farrow, C. E.G. (Eds.), Dynamic Processes in Magmatic Ore Deposits and their Application in Mineral Exploration. Geological Association of Canada, pp. 69–106.
Barnes, S.J., Naldrett, A.J., 1986. Variations in platinum group element concentrations in the Alexo mine komatiite, Abitibi greenstone belt, northern Ontario. Geol. Mag. 123, 515–524.
Barnes, S.J., Ripley, E.M., 2016. Highly siderophile and strongly chalcophile elements in magmatic ore deposits. Rev. Mineral. Geochem. 81, 725–774.
Barnes, S.J., Makovicky, E., Makovicky, M., RoseHansen, J., KarupMoller, S., 1997. Partition coefficients for Ni, Cu, Pd, Pt, Rh, and Ir between monosulfide solid solution and sulfide liquid and the formation of compositionally zoned Ni-Cu sulfide bodies by fractional crystallization of sulfide liquid. Can. J. Earth Sci. 34, 366–374.
Barnes, S.J., Prichard, H.M., Cox, R.A., Fisher, P.C., Godel, B., 2008. The location of the chalcophile and siderophile elements in platinum-group element ore deposits (a textural, microbeam and whole rock geochemical study): implications for the formation of the deposits. Chem. Geol. 248, 295–317.
Barnes, S.J., Fisher, L.A., Godel, B., Pearce, M.A., Maier, W.D., Paterson, D., Howard, D. L., Ryan, C.G., Laird, J.S., 2016. Primary cumulus platinum minerals in the Monts de Cristal complex, Gabon: magmatic microenvironments inferred from high-definition X-ray fluorescence microscopy. Contrib. Mineral. Petrol. 171 (3), 1–18.
Barnes, S.J., Taranovic, V., Schoneveld, L.E., Mansur, E.T., Le Vaillant, M., Dare, S.A.S., Staude, S., Evans, N.J., Blanks, D., 2020. The occurrence and origin of pentlandite-chalcopyrite-pyrrhotite loop textures in magmatic Ni-Cu sulfide ores. Econ. Geol. 115, 1777–1798.
Barnes, S.J., Stanley, C.R., Taranovic, V., 2022. Compositions and Ni-Cu-platinum group element tenors of Nova-Bollinger ores with implications for the origin of Pt anomalies in platinum group element-poor massive sulfides. Econ. Geol. 117 (8), 1687–1707.
Bennett, S., Heyding, R., 1966. Arsenides of the transition metals: viii. some binary and ternary group viii diarsenides and their magnetic and electrical properties. Can. J. Chem. 44, 3017–3030.
BGMS (Bureau of Geological and Mineral Resources of Sichuan Province), 1982. Exploration Report of the Zhengziyanwuo and Yangliuping Pt–Ni Deposits. Geological Publishing House, Beijing, People's Republic of China, Danba, Sichuan (in Chinese).
Cabri, L.J., 1981. Platinum-group elements: mineralogy, geology, recovery. Montreal. Montreal. Can. Inst. Min. Metall. 23, 267 pages.
Cabri, L.J., 2002. The platinum-group minerals. In: Cabri, L. (Ed.), The Geology, Geochemistry, Mineralogy, Mineral Beneficiation of the Platinum-Group Elements, Can. Inst. Min., Metall. Petrol, 54, pp. 13–129.
Cabri, L.J., Laflamme, J.G., 1976. The mineralogy of the platinum-group elements from some copper-nickel deposits of the Sudbury area, Ontario. Econ. Geol. 71, 1159–1195.
Cabri, L.J., Laflamme, J.G., 1984. Mineralogy and distribution of platinum-group elements in mill products from Sudbury. Can. Mineral. 22, 521–542.
Cabri, L.J., McGachie, R., Bradley, A., 1981. Mineralogy and distribution of the platinum-group in mill samples from the Cu-Ni deposits of the Sudbury, Ontario area. In: McGachie, R.O., Bradley, A.G. (Eds.), Precious Metals. Pergamon press Ltd, pp. 23–34.
Cabri, L.J., Kelvin, M., Yang, Z., Jackson, S.E., Altun, O., 2017. Application of LA-ICP-MS trace-element analysis for precious metal deportment: a case study of the Kevitsa mine, Finland. Eur. J. Mineral. 29, 635–644.
Chen, L.M., Song, X.Y., Keays, R.R., Tian, Y.L., Wang, Y.S., Deng, Y.F., Xiao, J.F., 2013. Segregation and fractionation of magmatic Cu-Ni-PGE Sulfides in the Western Jinchuan Intrusion, Northwestern China: insights from platinum group element geochemistry. Econ. Geol. 108, 1793–1811.
Chen, L.-M., Song, X.-Y., Danyushevsky, L.V., Wang, Y.-S., Tian, Y.-L., Xiao, J.-F., 2015. A laser ablation ICP-MS study of platinum-group and chalcophile elements in base metal sulfide minerals of the Jinchuan Ni–Cu sulfide deposit, NW China. Ore Geol. Rev. 65, 955–967.
Coghill, B.M., Wilson, A.H., 1993. Platinum-group minerals in the Selukwe Subchamber, Great Dyke, Zimbabwe: implications for PGE collection mechanisms and post-formational redistribution. Mineral. Mag. 57 (389), 613–633.
Dare, S.A.S., Barnes, S.J., Prichard, H.M., 2010a. The distribution of platinum group elements (PGE) and other chalcophile elements among sulfides from the Creighton Ni–Cu–PGE sulfide deposit, Sudbury, Canada, and the origin of palladium in pentlandite. Mineral. Deposita 45, 765–793.
Dare, S.A.S., Barnes, S.J., Prichard, H.M., Fisher, P.C., 2010b. The timing and formation of platinum-group minerals from the Creighton Ni-Cu-platinum-group element sulfide deposit, Sudbury, Canada: early crystallization of PGE-rich sulfarsenides. Econ. Geol. 105, 1071–1096.
Dare, S.A.S., Barnes, S.J., Prichard, H., Fisher, P., 2011. Chalcophile and platinum-group element (PGE) concentrations in the sulfide minerals from the McCreedy East deposit, Sudbury, Canada, and the origin of PGE in pyrite. Mineral. Deposita 46, 381–407.
Distler, V.V., Sinyakova, E.F., Kosyakov, V.I., 2016. Behavior of noble metals upon fractional crystallization of copper-rich sulfide melts. Dokl. Earth Sci. 469, 811–814.
Djon, M.L.N., Barnes, S.J., 2012. Changes in sulfides and platinum-group minerals with the degree of alteration in the Roby, Twilight, and High Grade Zones of the Lac des Iles Complex, Ontario, Canada. Mineral. Deposita 47, 875–896.
Fonseca, R.O., Campbell, I.H., O'Neill, H.S.C., Fitzgerald, J.D., 2008. Oxygen solubility and speciation in sulphide-rich mattes. Geochim. Cosmochim. Acta 72 (11), 2619–2635.
González-Jiménez, J.M., Deditius, A., Gervilla, F., Reich, M., Suvorova, A., Roberts, M.P., Roqué, J., Proenza, J.A., 2018. Nanoscale partitioning of Ru, Ir, and Pt in base-metal sulfides from the Caridad chromite deposit, Cuba. Am. Mineral. 103, 1208–1220.
González-Jiménez, J.M., Roqué-Rosell, J., Jiménez-Franco, A., Tassara, S., Nieto, F., Gervilla, F., Baurier, S., Proenza, J.A., Saunders, E., Deditius, A.P., Schilling, M., Corgne, A., 2019. Magmatic platinum nanoparticles in metasomatic silicate glasses and sulfides from Patagonian mantle xenoliths. Contrib. Mineral. Petrol. 174, 47.
Hanley, J.J., 2005. The aqueous geochemistry of the platinum-group elements (PGE) in surficial, low-T hydrothermal and high-T magmatic-hydrothermal environments. In: Short Course Series-Mineralogical Association of Canada, 35, pp. 35–56.
Hansen, M., Anderko, K., Salzberg, H., 1958. Constitution of binary alloys. J. Electrochem. Soc. 105, 260C–261C.
Harvey, J., Day, J.M.D., 2016. Introduction to highly siderophile and strongly chalcophile elements in high temperature geochemistry and cosmochemistry. Rev. Mineral. Geochem. 81, iii–xiv.
Helmy, H.M., Bragagni, A., 2017. Platinum-group elements fractionation by selective complexing, the Os, Ir, Ru, Rh-arsenide-sulfide systems above 1020°C. Geochim. Cosmochim. Acta 216, 169–183.
Helmy, H.M., Ballhaus, C., Wohlgemuth-Ueberwasser, C., Fonseca, R.O.C., Laurenz, V., 2010. Partitioning of Se, As, Sb, Te and Bi between monosulfide solid solution and sulfide melt - Application to magmatic sulfide deposits. Geochim. Cosmochim. Acta 74, 6174–6179.
Helmy, H.M., Ballhaus, C., Fonseca, R.O., Wirth, R., Nagel, T., Tredoux, M., 2013. Noble metal nanoclusters and nanoparticles precede mineral formation in magmatic sulphide melts. Nat. Commun. 4, 2405.
Helmy, H.M., Botcharnikov, R., Ballhaus, C., Deutsch-Zemlitskaya, A., Wirth, R., Schreiber, A., Buhre, S., Häger, T., 2020. Evolution of magmatic sulfide liquids: how and when base metal sulfides crystallize? Contrib. Mineral. Petrol. 176, 107.
Helmy, H.M., Botcharnikov, R., Ballhaus, C., Wirth, R., Schreiber, A., Buhre, S., 2023. How Pt and Pd are hosted in magmatic sulfides, substitutions and/or inclusions? Contrib. Mineral. Petrol. 178 (7), 41.
Holwell, D.A., McDonald, I., Armitage, P.E.B., 2006. Platinum-group mineral assemblages in the Platreef at the Sandsloot Mine, northern Bushveld Complex, South Africa. Mineral. Mag. 70 (1), 83–101.
Holwell, D.A., Adeyemi, Z., Ward, L.A., Smith, D.J., Graham, S.D., McDonald, I., Smith, J.W., 2017. Low temperature alteration of magmatic Cu-Ni-PGE sulfides as a source for hydrothermal Ni and PGE ores: a quantitative approach using automated mineralogy. Ore Geol. Rev. 91, 718–740.
Hutchinson, D., Kinnaird, J., 2005. Complex multistage genesis for the Ni–Cu–PGE mineralisation in the southern region of the Platreef, Bushveld Complex, South Africa. Appl. Earth Sci. 114, 208–224.
Hutchinson, D., McDonald, I., 2008. Laser ablation ICP-MS study of platinum-group elements in sulphides from the Platreef at Turfspruit, northern limb of the Bushveld Complex, South Africa. Mineral. Deposita 43 (6), 695–711.
Junge, M., Wirth, R., Oberthür, T., Melcher, F., Schreiber, A., 2014. Mineralogical siting of platinum-group elements in pentlandite from the Bushveld Complex, South Africa. Mineral. Deposita 50, 41–54.
Junge, M., Oberthür, T., Kraemer, D., Melcher, F., Piña, R., Derrey, I.T., Manyeruke, T., Strauss, H., 2019. Distribution of platinum-group elements in pristine and near-surface oxidized Platreef ore and the variation along strike, northern Bushveld Complex, South Africa. Mineral. Deposita 54, 885–912.
Kamenetsky, V.S., Zelenski, M., 2020. Origin of noble-metal nuggets in sulfide-saturated arc magmas: a case study of olivine-hosted sulfide melt inclusions from the Tolbachik volcano (Kamchatka, Russia). Geology 48, 620–624.
Keays, R.R., 1995. The role of komatiitic and picritic magmatism and S-saturation in the formation of ore-deposits. Lithos 34, 1–18.
Keays, R.R., Crocket, J.H., 1970. A study of precious metals in the Sudbury nickel irruptive ores. Econ. Geol. 65 (4), 438–450.
Kosler, J., 2001. Laser-ablation ICPMS study of metamorphic minerals and processes. In: Sylvester, P.J. (Ed.), Laser-Ablation-ICPMS in the Earth Sciences : Principles and Applications. Mineralogical Association of Canada Short Course Handbook, Ottawa, pp. 185–202.
Li, Y., Audétat, A., 2012. Partitioning of V, Mn, Co, Ni, Cu, Zn, As, Mo, Ag, Sn, Sb, W, Au, Pb, and Bi between sulfide phases and hydrous basanite melt at upper mantle conditions. Earth Planet. Sci. Lett. 355-356, 327–340.
Li, C., Barnes, S.J., Makovicky, E., RoseHansen, J., Makovicky, M., 1996. Partitioning of nickel, copper, iridium, rhenium, platinum, and palladium between monosulfide solid solution and sulfide liquid: Effects of composition and temperature. Geochim. Cosmochim. Acta 60 (7), 1231–1238.
Li, Y.Z., Mungall, J.E., 2022. Chalcophile element heterogeneity in Ni-Cu-(platinum group element) Orebodies of Raglan Horizon in Cape smith belt: implications for ore-forming processes. Econ. Geol. 117, 1131–1148.

Liang, Q.-L., Song, X.-Y., Wirth, R., Chen, L.-M., Dai, Z.-H., 2019. Implications of nano- and micrometer-size platinum-group element minerals in base metal sulfides of the Yangliuping Cu-Ni-PGE sulfide deposit, SW China. Chem. Geol. 517, 7–21.
Liang, Q.-L., Song, X.-Y., Wirth, R., Chen, L.-M., Yu, S.-Y., Krivolutskaya, N.A., Dai, Z.-H., 2022. Thermodynamic conditions control the valences state of semimetals thus affecting the behavior of PGE in magmatic sulfide liquids. Geochim. Cosmochim. Acta 321, 1–15.
Liu, Y.N., Brenan, J., 2015. Partitioning of platinum-group elements (PGE) and chalcogens (Se, Te, As, Sb, Bi) between monosulfide-solid solution (MSS), intermediate solid solution (ISS) and sulfide liquid at controlled fO(2)-fS(2) conditions. Geochim. Cosmochim. Acta 159, 139–161.
Liu, Y., Mungall, J.E., Ames, D.E., 2016. Hydrothermal redistribution and local enrichment of platinum group elements in the Tootoo and mequillon magmatic sulfide deposits, South Raglan Trend, Cape Smith Belt, New Quebec Orogen. Econ. Geol. 111, 467–485.
Longerich, H.P., Jackson, S.E., Günther, D., 1996. Inter-laboratory note. Laser ablation inductively coupled plasma mass spectrometric transient signal data acquisition and analyte concentration calculation. J. Anal. At. Spectrom. 11, 899–904.
Maier, W.D., Rasmussen, B., Fletcher, I.R., Godel, B., Barnes, S.J., Fisher, L.A., Yang, S.H., Huhma, H., Lahaye, Y., 2015. Petrogenesis of the ~2·77 Ga Monts de Cristal complex, Gabon: evidence for direct precipitation of Pt-arsenides from basaltic magma. J. Petrol. 56 (7), 1285–1308.
Makovicky, E., 2002. Ternary and quaternary phase systems with PGE. In: Cabri, L.J. (Ed.), Geology, Geochemistry, Mineralogy and Mineral Beneficiation of Platinum-group Elements, 54. Can. Inst. Min., Metall. Petrol, pp. 131–175.
Makovicky, M., Makovicky, E., Rose-Hansen, J., 1986. Experimental studies on the solubility and distribution of platinum group elements in base-metal sulphides in platinum deposits. In: Gallagher, M.J., Ixer, R.A., Neary, C.R., Prichard, Margaret, H. (Eds.), Metallogeny of Basic and Ultrabasic Rocks. Inst. Min. Metall, London, pp. 415–425.
Mansur, E.T., Barnes, S.J., Duran, C.J., 2019a. Textural and compositional evidence for the formation of pentlandite via peritectic reaction: implications for the distribution of highly siderophile elements. Geology 47, 351–354.
Mansur, E.T., Barnes, S.J., Duran, C.J., Sluzhenikin, S.F., 2019b. Distribution of chalcophile and platinum-group elements among pyrrhotite, pentlandite, chalcopyrite and cubanite from the Noril'sk-Talnakh ores: implications for the formation of platinum-group minerals. Mineral. Deposita 55, 1215–1232.
Mansur, E., Barnes, S.J., Ferreira Filho, C.F., 2021. The effects of post-cumulus alteration on the distribution of chalcophile elements in magmatic sulfide deposits and implications for the formation of low-S-high-PGE zones: the Luanga deposit, Carajás Mineral Province, Brazil. Can. Mineral. 59, 1453–1484.
Mcdonald, I., 2008. Platinum-group element and sulphide mineralogy in ultramafic complexes at western Andriamena, Madagascar. Appl. Earth Sci. 117 (1), 1–10.
McDonough, W.F., Sun, S.S., 1995. The composition of the Earth. Chem. Geol. 120, 223–253.
Mengason, M.J., Piccoli, P.M., Candela, P., 2010. An evaluation of the effect of copper on the estimation of sulfur fugacity (fs_2) from pyrrhotite composition. Econ. Geol. 105 (6), 1163–1169.
Mungall, J.E., Brenan, J.M., 2014. Partitioning of platinum-group elements and Au between sulfide liquid and basalt and the origins of mantle-crust fractionation of the chalcophile elements. Geochim. Cosmochim. Acta 125, 265–289.
Mungall, J.E., Andrews, D.R.A., Cabri, L.J., Sylvester, P.J., Tubrett, M., 2005. Partitioning of Cu, Ni, Au, and platinum-group elements between monosulfide solid solution and sulfide melt under controlled oxygen and sulfur fugacities. Geochim. Cosmochim. Acta 69, 4349–4360.
Naldrett, A.J., 2004. Magmatic Sulfide Deposits : Geology, Geochemistry, and Exploration. Springer, Berlin.
Naldrett, A.J., Lightfoot, P.C., Fedorenko, V.A., Doherty, W., Gorbachev, N.S., 1992. Geology and geochemistry of intrusions and flood basalts of the Noril'sk region, USSR, with implications for the origin of the Ni-Cu ores. Econ. Geol. 335 (4), 975–1004.
Naldrett, A.J., Fedorenko, V.A., Asif, M., Lin, S., Kunilov, V.E., Stekhin, A.I., Lightfoot, P. C., Gorbachev, N.S., 1996. Controls on the composition of Ni-Cu sulfide deposits as illustrated by those at Noril'sk, Siberia. Econ. Geol. 91 (4), 751–773.
O'Driscoll, B., González-Jiménez, J.M., 2016. Petrogenesis of the platinum-group minerals. Rev. Mineral. Geochem. 81 (1), 489–578.
Ohnenstetter, M., Johan, Z.K., Cocherie, A., Fouillac, C., Ohnenstetter, D., Chaussidon, M., Rouer, O., Makovicky, E., Makovicky, M., Karup-moller, S., Vaughan, D.J., Turner, G., Pattrick, R.A.D., Giże, A.P., Lyon, I.C., McDonald, I., 1999. New exploration methods for platinum and rhodium deposits poor in base-metal sulphides, 0371-7453 (108), B119–B150.
Park, J.-W., Campbell, I.H., Arculus, R.J., 2013. Platinum-alloy and sulfur saturation in an arc-related basalt to rhyolite suite: evidence from the Pual Ridge lavas, the Eastern Manus Basin. Geochim. Cosmochim. Acta 101, 76–95.
Pina, R., Gervilla, F., Barnes, S.J., Ortega, L., Lunar, R., 2013. Platinum-group elements-bearing pyrite from the Aguablanca Ni-Cu sulphide deposit (SW Spain): a LA-ICP-MS study. Eur. J. Mineral. 25, 241–252.
Power, M.R., Pirrie, D., Jedwab, J., andStanley C. J., 2004. Platinum-group element mineralization in an As-rich magmatic sulphide system, Talnotry, Southwest Scotland. Mineral. Mag. 68 (2), 395–411.
Prichard, H.M., Fisher, P.C., McDonald, I., Knight, R.D., Sharp, D.R., Williams, J.P., 2013a. The distribution of PGE and the role of arsenic as a collector of PGE in the spotted Quoll nickel ore deposit in the Forrestania Greenstone Belt, Western Australia. Econ. Geol. 108 (8), 1903–1921.
Prichard, H.M., Knight, R.D., Fisher, P.C., McDonald, I., Zhou, M.F., Wang, C.Y., 2013b. Distribution of platinum-group elements in magmatic and altered ores in the Jinchuan intrusion, China: an example of selenium remobilization by postmagmatic fluids. Mineral. Deposita 48, 767–786.
Putnis, A., 1992. An Introduction to Mineral Sciences. Cambridge University Press, New York.
Qi, L., Gao, J.F., Huang, X.W., Hu, J., Zhou, M.F., Zhong, H., 2011. An improved digestion technique for determination of platinum group elements in geological samples. J. Anal. At. Spectrom. 26, 1900–1904.
Savard, D., Barnes, S.-J., Meisel, T., 2010. Comparison between nickel-sulfur fire assay Te Co-precipitation and isotope dilution with high-pressure asher acid digestion for the determination of platinum-group elements, rhenium and gold. Geostand. Geoanal. Res. 34, 281–291.
Sinyakova, E.F., Kosyakov, V.I., 2012. The behavior of noble-metal admixtures during fractional crystallization of As- and Co-containing Cu–Fe–Ni sulfide melts. Russ. Geol. Geophys. 53, 1055–1076.
Smith, J.M., Ripley, E.M., Li, C.S., Shirey, S.B., Benson, E.K., 2022. Magmatic origin for the massive sulfide ores in the sedimentary country rocks of mafic-ultramafic intrusions in the Midcontinent Rift System. Mineral. Deposita 57, 1189–1210.
Song, X.Y., 2004. Geochemistry of Permian Flood Basalts and Related Ni-Cu-(PGE) Sulfide-Bearing Sills in Yangliuping, Sichuan Province, China. Ph. D. thesis,. Univ. of Hong Kong.
Song, X.Y., Zhou, M.F., Hou, Z.Q., Cao, Z.M., Wang, Y.L., Li, Y.G., 2001. Geochemical constraints on the mantle source of the upper permian Emeishan continental flood basalts, southwestern China. Int. Geol. Rev. 43, 213–225.
Song, X.Y., Zhou, M.F., Cao, Z.M., Sun, M., Wang, Y.L., 2003. Ni-Cu-(PGE) magmatic sulfide deposits in the Yangliuping area, Permian Emeishan Igneous province, SW China. Mineral. Deposita 38, 831–843.
Song, X.Y., Zhou, M.F., Cao, Z.M., 2004. Genetic relationships between base-metal sulfides and platinum-group minerals in the Yangliuping Ni-Cu-(PGE) sulfide deposit, southwestern China. Can. Mineral. 42, 469–483.
Song, X.Y., Zhou, M.F., Tao, Y., Xiao, J.F., 2008. Controls on the metal compositions of magmatic sulfide deposits in the Emeishan large igneous province, SW China. Chem. Geol. 253, 38–49.
Song, X.Y., Keays, R.R., Zhou, M.F., Qi, L., IhIenfeld, C., Xiao, J.F., 2009. Siderophile and chalcophile elemental constraints on the origin of the Jinchuan Ni-Cu-(PGE) sulfide deposit, NW China. Geochim. Cosmochim. Acta 73, 404–424.
Song, X.Y., Qi, H.W., Hu, R.Z., Chen, L.M., Yu, S.Y., Zhang, J.F., 2013. Formation of thick stratiform Fe-Ti oxide layers in layered intrusion and frequent replenishment of fractionated mafic magma: evidence from the Panzhihua intrusion, SW China. Geochem. Geophys. Geosist. 14, 712–732.
Su, S., Li, C., Zhou, M.-F., Ripley, E.M., Qi, L., 2008. Controls on variations of platinum-group element concentrations in the sulfide ores of the Jinchuan Ni-Cu deposit, western China. Mineral. Deposita 43, 609–622.
Tao, Y., Li, C., Hu, R., Ripley, E.M., Du, A., Zhong, H., 2007. Petrogenesis of the Pt-Pd mineralized Jinbaoshan ultramafic intrusion in the Permian Emeishan Large Igneous Province, SW China. Contrib. Mineral. Petrol. 153, 321–337.
Tao, Y., Li, C., Song, X.-Y., Ripley, E.M., 2008. Mineralogical, petrological, and geochemical studies of the Limahe mafic–ultramatic intrusion and associated Ni–Cu sulfide ores, SW China. Mineral. Deposita 43, 849–872.
Toulmin, P., Barton, P.B., 1964. A thermodynamic study of pyrite and pyrrhotite. Geochim. Cosmochim. Acta 28 (5), 641–671.
Tredoux, M., Lindsay, N.M., Davies, G., Nald, I., 1995. The fractionation of platinum-group elements in magmatic systems, with the suggestion of a novel causal mechanism. S. Afr. J. Geol. 98, 157–167.
Waal, S.A.D., Xu, Z.G., Li, C.S., Mouri, H., 2004. Emplacement of viscous mushes in the Jinchuan ultramafic intrusion, western China. Can. Mineral. 42 (2), 371–392.
Wang, C.Y., Zhou, M.F., 2006. Genesis of the Permian Baimazhai magmatic Ni–Cu–(PGE) sulfide deposit, Yunnan, SW China. Mineral. Deposita 41, 771–783.
Wang, C.Y., Prichard, H.M., Zhou, M.-F., Fisher, P.C., 2008. Platinum-group minerals from the Jinbaoshan Pd–Pt deposit, SW China: evidence for magmatic origin and hydrothermal alteration. Mineral. Deposita 43, 791.
Wirth, R., Reid, D., Schreiber, A., 2013. Nanometer-sized platinum-group minerals (PGM) in base metal sulfides: new evidence for an orthomagmatic origin of the Merensky Reef PGE ore deposit, Bushveld Complex, South Africa. Can. Mineral. 51, 143–155.
Wood, S.A., 2002. The aqueous geochemistry of the platinum-group elements with applications to ore deposits. In: Cabri, L.J. (Ed.), The Geology, Geochemistry, Mineralogy, Mineral Beneficiation of the Platinum-Group Elements, 54. Can. Inst. Min., Metall. Petrol, pp. 211–250.
Xu, Y., Chung, S.-L., Jahn, B.-M., Wu, G., 2001. Petrologic and geochemical constraints on the petrogenesis of Permian–Triassic Emeishan flood basalts in southwestern China. Lithos 58, 145–168.
Yudovskaya, M.A., Kinnaird, J.A., Grobler, D.F., Costin, G., Abramova, V.D., Dunnett, T., Barnes, S.-J., 2017. Zonation of Merensky-style platinum-group element mineralization in Turfspruit Thick Reef Facies (Northern Limb of the Bushveld Complex). Econ. Geol. 112 (6), 1333–1365.
Zhang, M., Li, Y., 2021. Breaking of Henry's law for sulfide liquid–basaltic melt partitioning of Pt and Pd. Nat. Commun. 12 (1), 5994.
Zhong, H., Zhou, X.H., Zhou, M.F., Sun, M., Liu, B.G., 2002. Platinum-group element geochemistry of the Hongge Fe-V-Ti deposit in the Pan-Xi area, southwestern China. Mineral. Deposita 37, 226–239.